ORNL/TM-2023/2848

Study on Electrostatic Separation of Quinoline Insolubles from Coal Tar Pitch

Hong Wang
Eric Wolfe
Edgar Lara-Curzio
Marco Martinez
Tracie Lowe

March 2023

OAK RIDGE National Laboratory

ORNL IS MANAGED BY UT-BATTELLE LLC FOR THE US DEPARTMENT OF ENERGY

ORNL/TM-2023/2848

Materials Science and Technology Division

STUDY ON ELECTROSTATIC SEPARATION OF QUINOLINE INSOLUBLES FROM COAL TAR PITCH

Hong Wang, Eric Wolfe, Edgar Lara-Curzio, Marco Martinez,
Tracie Lowe

March 2023

Prepared by
OAK RIDGE NATIONAL LABORATORY
Oak Ridge, TN 37831
managed by
UT-BATTELLE LLC
for the
US DEPARTMENT OF ENERGY
under contract DE-AC05-00OR22725

CONTENTS

LIST OF FIGURES

LIST OF TABLES

ABBREVIATIONS

ASTM	ASTM International (formerly American Society for Testing and Materials)
BGL	Blue Gem coal liquid
BTX	benzene toluene xylene
CFTF	Carbon Fiber Technology Facility
CN	category number
CTP	coal tar pitch
DE	diatomaceous earth
DEP	dielectrophoresis
DOE	US Department of Energy
EDS	energy dispersive spectroscopy
EP	electrophoresis
ESP	electrostatic precipitation
ESS	electrostatic separation
ETH	ethanol
FCCS	fluid catalytic cracking slurry
GRD	ground
HV	high-voltage
ID	inside diameter
IR	inner radius
OC	open circuit
OD	outside diameter
ORNL	Oak Ridge National Laboratory
PVA	polyvinyl alcohol
PVC	polyvinyl chloride
QI	quinoline insoluble
QS	quinoline soluble
RE	removal efficiency
RT	room temperature
SC	short circuit
SEM	scanning electron microscopy
SN	serial number
SP	softening point
SSL	stainless steel
TG	thermogravimetric
TI	toluene insoluble
TN	test number
TP	temperature
TS	toluene soluble
XRD	X-ray diffraction

ACKNOWLEDGEMENTS

The work was funded by the US Department of Energy (DOE) Fossil Energy and Carbon Management program under DOE contract DE-AC05-00OR22725 with UT-Battelle, LLC.

Authors appreciate many individuals of DOE's Oak Ridge National Laboratory (ORNL) for their helpful discussion and great support. Particularly, we would like to thank Caitlin Duggan for preparing scanning electron microscopy samples, April Case and Blake Henry for reviewing test setup, and Aparna Annamraju for processing of coal tar pitch samples. Authors are grateful to Erica Heinrich for editing this report and many helpful suggestions.

Authors also want to thank Drs. Chanaka Ihala Gamaralalage and Georgios Polyzos of ORNL for their review and constructive comments.

EXECUTIVE SUMMARY

The feasibility of electrical separation in the removal of quinoline insoluble (QI) particles from coal tar pitch (CTP) was experimentally investigated. QI particle involvement prohibits the effective fabrication of high-quality value-added products, such as carbon fibers, from CTP. A substantial and sustainable CTP market exists around the world; therefore, a strong incentive exists to develop a viable technical approach to effectively and economically remove QI particles from CTP. The electrical separation method shows promise to achieve this technical goal (Cao et al., 2012).

Even with the given setup (wire- cylinder adapted), critical issues remain to be addressed for this method to be applicable to the CTP: (1) identifying the wash oil used in the original QI separation, (2) understanding the mechanism of QI separation, (3) characterizing the deposit, and (4) identifying the QI.

This study integrated a set of experimental and analysis techniques into the electrical separation tests to address the aforementioned issues.

1. An extensive search was performed, and nine original solvents were identified for subject CTPs. The electrical separation tests and/or electrical resistance measurement preliminarily screened the list down to toluene, wash oil, carbon disulfide, and benzene for a single-part solvent. The search was further extended to include two-part mixtures (quinoline and toluene, quinoline and US wash oil, carbon disulfide and toluene), and three-part mixtures (Blue Gem coal liquid, benzene toluene xylene (BTX), and ethanol; wash oil, BTX, and ethanol).
2. The test setup was modified and adapted to enhance electric field and deposit collection with the given high-voltage capability, and to examine the deposit direction as related to electric field. Two sizes of glass beaker and three collection rod configurations were attempted.
3. An extensive literature survey identified the solids and liquids for the electrical separation modeling system. Three solids and two liquids were identified and examined with both the nominal electric field and the revered electric field to develop the understanding of electrical separation mechanism.
4. QI was extracted from the subject CTPs and from the deposits by using the procedure based on ASTM Standard D2318-20 to evaluate the removal efficiency of QI particles.
5. Scanning electron microscopy (SEM) and energy dispersive spectroscopy (EDS) were performed to analyze the chemical compositions of the deposit and of the QI extracts from the deposit and CTPs.

Key findings are as follows:

1. Electric current responses
    - The electric current level of the CTP–wash oil solution reported by Cao et al. (2012) can be attained by using a mixture of 25% quinoline and 75% toluene for the CTPs examined in this study under the same electrical load condition.
    - The electric current tends to decrease during the test period because of the decreasing number of charged particles.
    - The reversed field corresponded to the configuration of electrostatic precipitation for positive corona discharge. The high electric field can result in dielectric breakdown and lead to an abrupt current surge.

2. Deposit response and solvent candidates
    - Deposit of particles in CTP mixture can be effectively implemented in a wire-cylinder configuration as proposed and examined in this study.

- Deposit depends on the solvents. Among the solvents tested, two- and three-part solvents that included quinoline and ethanol (i.e., 25% quinoline and 75% toluene; 50% quinoline and 50% toluene; and 33% wash oil, 33% BTX, and 34% ethanol) produced the highest deposit weight
- The deposit process examined in this study is derived from the charged particles. An appreciable relation exists between deposit weight and electric charge.

3. QI removal efficiency (RE)

    - The RE of the electrostatic separation can reach as high as 76.2% for Carbores, and 61.6% for Koppers.
    - The RE can be further enhanced if the field level increases from 0.16 kV/mm that was used in the current study to 0.23 kV/mm, according to the relation established between the RE and the electric field.

4. Testing of the modeling system

    - The motion of particles is originally driven by the charge-based electric force in the cases tested. The solid particle separation mechanism is similar to that of QI deposition in CTP.
    - The mechanical movement of solid particles can be strongly affected by the gravitational and viscous forces in the electric field.

5. EDS analysis and chemical compositions

    - The main chemical composition of deposit QI matches that of as-prepared CTP QI. The deposit QI is derived from the same group of the CTP QI.
    - In addition to carbon, the QI contains oxygen, sodium, aluminum, silicon, iron, and sulfur.

The work for the near future is also discussed.

1. INTRODUCTION

1.1 SIGNIFICANCE OF QI SEPARATION

Coal tar pitch (CTP), a byproduct from processing of coal tar, accounts for about 2.4–3.6 wt % of the total output of coke. CTP has a high carbon content and can be used in the fabrication of various advanced carbon materials, such as needle coke, carbon fibers, and mesocarbon microbeads.[1-4] Worldwide coke production reached 639 Mt in 2018 and has remained around this level since then.[5] Thus, the CTP market size is about 19 Mt. Tremendous motivation exists for employing CTP for added-value products and environment protection.

However, CTP cannot be directly used because quinoline insoluble (QI) particles and ash are present. The involvement of QI particles with CTP delays the commencement of sphere generation and increases the time required to generate spherules of mesophase in the carbonization process, as illustrated by Moriyama et al.[6] The treatment of CTP, particularly the removal of QI and ash, is crucial to manufacturing carbon composites. The effect of QI on the quality of carbon materials has been addressed in several publications: for example, Stadelhofer et al.,[7] Zhu et al.,[8,9] An et al.,[10] and Lei et al.[11]

1.2 TECHNICAL CHALLENGE

Four methods are currently used for removing QI particles: filtering, gravitational settling with a solvent, the centrifugal method, and the extraction method.

The main disadvantages of these methods include high labor intensity and arduous work, as critically reviewed by Yu et al.[12] For example, filtering requires fine screening and relatively high temperatures of 140°C–200°C. The procedural steps are inconvenient, and the recovery rate is only about 70 wt %. Gravitational settling with a solvent requires long periods of time to complete, usually more than 24 h, at some minimal temperature. The boundary between the solution and precipitates is unclear and cannot be specifically determined because the solution is black. Centrifugation and extraction are completed relatively rapidly but consume large amounts of energy. Treatment difficulties arise when a large volume of raw material must be purified.

1.3 APPROACH

Electrostatic separation of ash has emerged as a new method to remove QI particles from coal tar. Recently, Cao et al.[13] investigated such method for the simultaneous removal of QI particles and ash, and demonstrated that the new method consumed only 12% of the energy of the centrifugal method.

The present work studied electrostatic separation as a method to remove QI particles from coal tar pitch and investigated the applicability of this method to various candidates to ensure the availability of high-quality coal tar pitch for downstream carbon fiber processing.

2. BACKGROUND

2.1 ELECTRICAL SEPARATION OF SOLID–LIQUID MIXTURE

2.1.1 Charge-Based Electrostatic Precipitation

The electrostatic separation (ESS) process uses electric force to separate particles or droplets from a mixture of solid/liquid and gas phases. In a variety of applications, the original electric force is based on Coulomb's law:

$$F = qE, \tag{1}$$

where F is the Coulomb force, q is the electric charge, and E is the electric field. The Coulomb force can be used to determine the motion of particles for the separation along with other critical factors, including gravitational and drag forces.

The two typical configurations employed in an electrostatic separator are wire–plate and wire–cylinder. In the wire–plate configuration, a wire is set parallel to the plate; the wire serves as a high-voltage (HV) electrode or discharge electrode, and the plate serves as a ground (GRD) and collecting electrode. The mixture is injected and flows through the space between the electrodes. Under energized conditions, a corona discharge can be created near the curved electrode where the potential gradient is extremely high, ionizing the fluid medium. Beyond the discharge zone, the suspended particles are charged by the unipolar ions from the discharge and are driven to the plate electrode. The principles governing the operation of electrostatic separation can be found in the literature: for example, White [14] and Chang et al.[15]

Extensive experimental studies were dedicated to investigating various stages of ESP, including the corona discharge,[16, 17] particle charging,[18, 19] particle motion[20] and particle collection.[21-23] At the same time, analytical and numerical studies were also conducted to understand the mechanisms associated with the ESP process, as reviewed by Long and Yao.[24]

In the aerosol community, the electrostatic process using charge as a driving element to achieve particle separation is usually called electrostatic precipitation (ESP). Overall, ESP has been developed to a mature technology and has been widely applied in the aerosol field since Cottrell's demonstration.[25] Many successful case studies can be found in Yan.[26]

2.1.2 Dipole-Based Electrostatic Separation (ESS)

Another electric force stems from the dipole. The particles in the mixture are neutral. To be activated under an electric field, the particles should comprise polar materials. The positive and negative ions or electron clouds are displaced either permanently or temporally. The electric force F on a dipole μ in a nonuniform field E can be calculated using Eq. (2):

$$F = \mu \cdot \nabla E. \tag{2}$$

As can be seen, the dipole-based electric force is associated with the nonuniform electric field where the field gradient dominates the particle movements. Once the dipole aligns with an electric field, the particle moves in the direction of the electric field's gradient. With respect to the effect of electric field, this motion is different from the charge-based force, in which the particle's direction depends on the polarity of charge with the particle.

Several configurations can be used to create a nonuniform field, including wire–plate, wire–cylinder, and wire–wire. For analytical purposes, the electric field distribution in these setups can be approximated by that of the wire–cylinder configuration. The detailed study showed that, for a wire–cylinder configuration, the electric force experienced by the dipole depends on the gradient of squared absolute of field along with other factors, including particle size, dielectric constants of dispersing and dispersed phases of the mixture:

$$F = 2\pi {r_\mathrm{p}}^3 \mu_K \nabla |E|^2, \quad (3)$$

where E is the root mean square of electric field, r_p is the particle radius, and μ_K is the factor with the dielectric constants of liquid and solid phases. The implication of Eq. (3) is that the direction of electric force shall be toward the area where the gradient of the absolute of electric field is the highest (i.e., the wire electrode). The motion of particles is termed as dielectrophoresis (DEP) for the case in which the electric force is based on dipole. The case in which the force is based on charge is termed as electrophoresis (EP). The governing principles of DEP can be found in the literature by Pohl,[27, 28] Pohl and Schwar.[29]

The DEP has been studied for various liquid–solid mixtures, including plastic, coal, and ceramics in many different solvents,[27, 28] and single particles of various materials in ionic liquids.[30-32] The experimental setups were types of wire–cylinder, wire–plate and wire–wire, as summarized in Table 1.

Table 1. Existing test setups used in laboratory studies for electrical separation, without bed

No.	Electric setup (separator)	Temperature	Time	Ref.
1	Center electrode: (1) 0.25 mm diameter, oxide-coated tungsten wire; (2) uninsulated copper wire. Outer electrode: 8 mm height tin foil band resting on the inner wall of 10 cm diameter Petri dish. 10 kV	Gentle heating	Several minutes	27
2	(1) Center electrode: Teflon coated wire; (2) outer electrode: Pyrex tube with 20 mm inside diameter; 4 kV AC, 60 Hz			27
3	(1) Center electrode: 0.25–3.0 mm diameter, insulation covered or bare; (2) outer electrode: Pyrex tube uncoated or coated with graphite, 11–20 mm diameter; (3) 10 kV AC/DC	RT	3 min; 12.5 mL/min	28
4	Wire–plate cell, wire separation 2 mm; AC 200 V, 1 kHz, 20 kHz, and 2.55 MHz			30
5	Wire–plate cell, wire separation 2 mm; AC 200 V, 1 kHz, 20 kHz, and 2.55 MHz			31
6	Wire–wire cell, wire separation 2 mm; AC 120 V, 100 kHz to 27 MHz		1 min	32
7	Inner copper rod 3 mm diam. 100 mm length; outer aluminum sheet resting against a 300 mL beaker; 3–9 kV	35°C	40 min	13

Note: RT: room temperature

A bed of glass and ceramic beads has been introduced and studied to increase the number of collecting points and the area of collection.[33] In this setup, the electrostatic separator is filled with spherical glass beads; the glass beads are dielectrics and, once polarized by an external field, can serve as the sources of a new nonuniform electric field. The solid particles in the mixture are adsorbed to the surface of the fillers under the action of the dielectrophoretical force, deposited, and subsequently washed.

The electrostatic separator equipped with a glass bed has been investigated in the separation of catalytical particles in a fluid catalytic cracking slurry (FCCS) by, for example, Fang et al.,[34- 36] Guo et al.,[37] and Li et al.[38, 39] To date, many sets of ESSs have been proposed or are running.[40, 41] Some laboratory setups that use glass beads are summarized in Table 2.

Table 2. Existing test setups used in laboratory studies for electrical separation, with bed

No.	Electric setup (separator)	Bed	Temperature	Time	Ref.
1	Cylinder, 5 cm diameter, 27 cm height, center rod diameter 2–6 mm; 8 kV	Bed same as cylinder, 27 cm; 3 or 6 mm diameter glass ball	RT	20 s; 18 cm^3/s	33
2	6 mm metal rod diameter, 50 mm steel tube diameter × 1.5 m length; 4.8 kV	Packing height 80 cm; 2–3 mm diameter, glass, ceramic, plastic	RT	single layer, 0.2–0.7 s	34
3	Separator, rectangular: 80 × 40 × 200 mm; electrode plates: 80 × 80 mm; 5–30 kV	Bed height unknown; 5–6 mm diameter glass balls	RT	1.5 min Q = 66 mL/min	35
4	Separator, cylinder: 50 mm diameter; center electrode rod 6 mm	Bed height 158 mm; 56 mm diameter glass balls	RT	1.5 min Q = 66 mL/min	35
5	Steel tube 124 mm diameter × 600 mm length; 20 kV	Packing height 220 mm; 5–6 mm diameter glass balls		18 min	36
6	6 mm HV copper rod diameter, 500 mm steel tube diameter; 9 kV; 0.36 kV/cm	Packing height 200 mm; glass ball size unknown	80°C	20 min	37
7	10 mm diameter HV copper rod, 75 mm diam × 200 mm length plexiglass tube; 1.5–9.75 kV/cm	Packing height 120 mm; 1.5–4 mm diameter glass balls	RT	20–40 min.	38
8	SSL, 120 mm diameter, 390 mm height; 2–12 kV	Packing height 75–300 mm; 3.5–4 mm diameter glass balls	RT	8 h, (1.58–3.17) × 10^{-6} m/s inlet velocity	39

Note: RT: room temperature

2.1.3 Solids for Modeling System

CTP is a complicated system, and the electrical separation can be quite involved because of the various components associated with CTP. The modeling system has been proposed to develop an understanding of underling mechanisms.

The modeling system comprises solid and liquid phases whose properties are well known and for which relevant data are established. A literature survey revealed that several systems have been proposed and used to study the electrical separation for various applications. These systems are summarized in Table 3.

Table 3. Literature survey on studied solid–liquid systems in electrical separation

No.	Solid	Liquid	Mixture	Ref.
1	(1) PVC, with carbon black filler; (2) PVC PVA copolymers, with carbon black	Di-isopropyl ketone	1 g solid in 50 mL liquid	27
2	(1) Coal dust, (2) charcoal dust	Toluene	1 g solid in 50 mL liqqid	27
3	PVC (4.6, polar)	1:1 volume mixture of carbon tetrachloride and benzene (dielectric constant 2.2, nonpolar)		27
4	PVC; 90–213 μm	Carbon tetrachloride and benzene (1:1)	10 vol %	28
5	Lead hafnate, quartz, silicon, stannic oxide, Sn, TiO_2	Salts: K^+, Ca^{2+}, La^{3+}, and Th^{4+} nitrates and K_2SO_4	Single suspended ball in solution	30
6	Silicon, silicon dioxide, tin, stannic oxide, rutile, lead halfnate	Dioxane–water mixture, 100% to 0% wt	Single suspended ball in solution	31
7	AgBr; pAg 4–7.2	Dioxane–water mixture, 100% to 20% wt		32
8	MgO, ilmenite ($FeTiO_2$), PVC, Cu;	Liquid kerosene	0.5 wt %	33
9	Diatomaceous earth, 30–75 μm;	(1) Alkylbenzene; (2) α-vinyl polymer; (4–7) × 10^{-2} Pa s	0.2 wt %	34
10	Diatomaceous earth, 10–30 μm;	Oil for steel cold work; mineral oil	0.3 wt %	35
11	Catalyst in FCCS	FCCS from two plants	0.077–0.503 wt %	37
12	Coal tar pitch	Washing oil	20 g/75 mL	13
13	(1) Catalyst in FCCS; (2) additives, R–CH = O, 1 wt %	FCCS from one plant	As-received	37
14	Catalyst for FCC, particle size 3–26 μm; usually made of zeolite	Alkylbenzene	2–6 g/L	38
15	Catalyst, particles 3 μm diameter, 1,027 kg/m^3; usually made of zeolite	Alkylbenzene	8 g/kg	39

2.2 TECHNICAL GAP

- The existing work in electrostatic separation study on CTP is apparently limited to the laboratory.
- The electrical separation of solid particles from a mixture of liquid and solid is sensitive to the dielectric properties of individual components. The application of this method was demonstrated in a single CTP system with one solvent. Thus, more tests using various candidate CTPs are needed to demonstrate feasibility.
- The electrical separation of solids from a liquid–solid mixture can be dominated by either DEP or EP. The previous study did not clarify the underlying mechanism. A thorough understanding of the separating mechanism not only verifies the effectiveness of this method but also offers a clear pathway to scale up the method.
- Although the deposits were analyzed and characterized using X-ray diffraction (XRD), thermal and elemental analysis methods, information about the molecular structures of the solid and liquid phases is not available.

2.3 THE OBJECTIVES

- Study the feasibility of electric separation of QI by using the existing HV capacity
- Develop understanding of electric separation mechanism

3. EXPERIMENTAL APPROACH

3.1 EXPERIMENTAL SETUP

3.1.1 Nominal Setup

The experimental setup used in this study is illustrated in Figure 1. A similar setup was also used in a previous study,[13] and it was adapted in the present work.

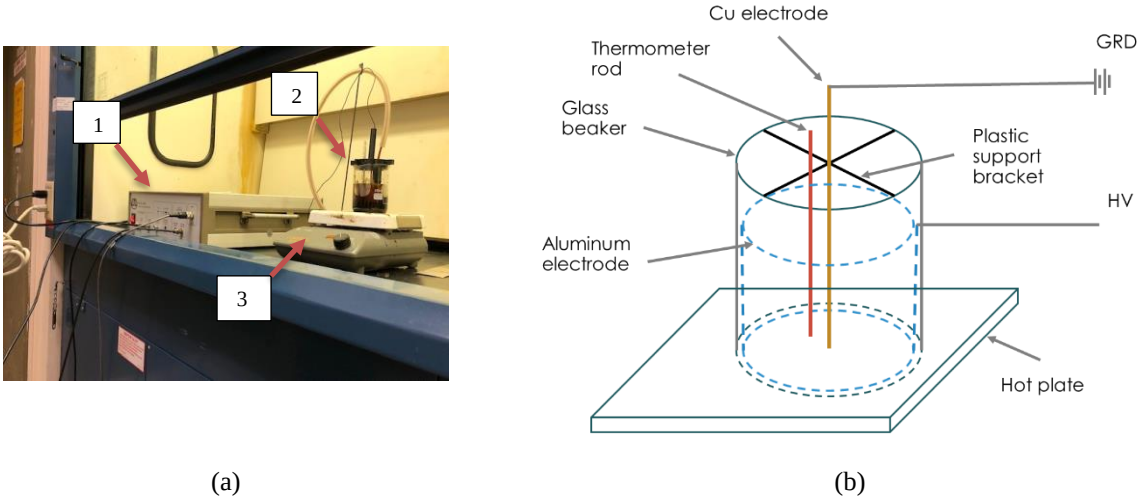

Figure 1. Experimental setup. (a) Image: 1—HV amplifier, 2—glass beaker with electrodes and thermometer, 3—hot plate. (b) Schematic.

A glass beaker containing the solution was placed on a hot plate. The beaker in the figure had a volume of 250 mL and an inside diameter of 65 mm. A copper rod of 3 mm diameter served as GRD electrode in the center; an aluminum sheet 2 in. (50.8 mm) wide and 1/32 in. (0.79 mm) thick, bent and formed to a circular shape, was set against the inner surface and bottom of the beaker. The circumferential length and width of the sheet were designed to make a closed circle or hollow cylinder and, when inserted, to contain the entire solution.

The metal sleeves were crimped and bolted to the GRD and HV cables for electrical connection. A 3D-printed plastic bracket guided the GRD wire, thermal meter rod, and HV cable. The bracket was designed to fit into the beaker, hold the rods/cable in place, and allow the solution to be poured through the opening. A button on the hot plate manually controlled the heating of the solution.

A Trek 609E-6 HV amplifier (Lockport, NY, USA; 4 kV, 20 mA) was used. The same amplifier was also employed in several high–electric field applications previously by Wang et al.[42-45] and Zhang et al.[46,47]

A LabView program was used to generate an input signal for the HV amplifier according to a predetermined waveform and to acquire the data, including monitoring amplifier voltage and current. The data communication between the amplifier and the LabView program was established using a NI USB-6251 I/O device along with an SCB-65 connection board. The program has a normal acquisition mode that can be used in the static test condition. The sampling rate was 10 Hz.

3.1.2 Modifications

Several modifications were made to the existing experimental setup.

3.1.2.1 Size of beaker

The experimental setup was modified to use a smaller beaker with an inner diameter of 54 mm. This smaller diameter generates a stronger electric field to the solution. The electric field was enhanced from 0.13 kV/mm in the nominal setup to 0.16 kV/mm for a maximum voltage of 4 kV. When the beaker diameter decreased, the solution height also changed. For the same amount of mixture, 70 mL liquid with 20 g of solid, the height increased from 26 to 38 mm.

3.1.2.2 Geometrical shape of electrode

To improve the deposit collection, a 3mm thick metal disk was attached to the lower end of the copper rod. Two diameters were attempted: 7.5 and 19.0 mm.

3.1.2.3 Reversed electric field

One of the modifications involved switching electrodes to investigate the effect of electrical direction on the deposit response. Namely, the center copper rod served as the HV electrode, and the side aluminum sheet served as the GRD electrode. This configuration switched the electrical direction from inward to outward. All the configurations tested are summarized in Table 4.

Table 4. Summary of setup configurations

Configuration	Beaker		Solution (70 mL)	Copper rod	Disk	Aluminum cylinder		Electric field (4kV)	
	Volume (mL)	Diameter (mm)	Height (mm)	Inside radius (mm)	Radius (mm)	Inside radius (mm)	Height (mm)	Strength (kV/mm)	Direction
LB1	250	65	26	1.59	NA	32.5	50.8	0.13	Inward
LB2	250	65	26	1.59	3.75	32.5	50.8	0.13	Inward
SB1	150	54	38	1.59	NA	27	50.8	0.16	Inward
SB2	150	54	38	1.59	3.75	27	50.8	0.16	Inward
SB3	150	54	38	1.59	9.50	27	50.8	0.16	Inward
SB4	150	54	38	1.59	3.75	27	50.8	0.16	Outward

3.2 TEST CONDITIONS

3.2.1 Temperature

Test temperature was set at 35°C.

3.2.2 Voltage Profile

The voltage profile consisted of increasing the voltage to 4 kV at 20 V/s in 200 s, 2,400 s (40 min) of constant voltage at 4 kV, and decreasing the voltage to 0 kV at 20 V/s in 200 s.

3.2.3 Electrode Variants

At the beginning, a Cu rod of constant diameter of 3 mm was used. To help capture the deposit, a small disk was attached as mentioned above to the lower end of rod. Disks of diameters of 7.5 and 19.0 mm were attempted. The small disk was used in most of the tests reported, and the large one was limited to one test.

3.2.4 Electric Field

Two electric field levels were examined: 0.13 and 0.16 kV/mm. For a given voltage of 4 kV, two different beaker sizes were used: 32.5 and 27 mm in diameter. These different sizes provided two electrode spacings for the two field levels.

Under nominal conditions, the center rod served as a GRD electrode, and the aluminum sheet served as an HV electrode. This nominal setting generated a field directed toward the center of beaker. In another case, the GRD and HV electrodes were switched, resulting in a field directed toward the outside of beaker.

3.3 MATERIALS

3.3.1 CTP

Several candidate CTPs were examined in this study, including Blue Gem, Springfield, Carbores, and Koppers. The CTPs were selected because of the current interest of industry or availability of data. All the materials were ground into mesh sizes 60, -80, -325, except one that was tested as tar. The items examined in this study are shown in Table 5 with a check mark (✓).

Table 5. Material conditions of CTPs used in electrical separation study

CTPs	Material format	Mesh 60	Mesh -80	Mesh -325	Vendor/supplier
Blue Gem	Powder	✓			
Carbores	Powder	✓	✓	✓	Rutgers/CFTF
Koppers	Powder	✓	✓	✓	
Springfield	Tar				Springfield Coal

Note: CFTF: Carbon Fiber Technology Facility

3.3.1.1 Solvents

A variety of candidate solvents were identified because of their application in laboratory studies and industry, as listed in Table 6. The table covers wide ranges of dielectric constants and boiling points. Toluene, wash oil, carbon disulfide, benzene, diesel, and benzene toluene xylene (BTX) all have a dielectric constant less than 2.6. Quinoline has the next largest dielectric constant at 8.89. Pyridine and ethanol have the largest dielectric constants: greater than 12.4.

Table 6. Candidate solvents studied for electrical separation

No.	Solvent	Boiling point (°C)	Dielectric constant	Polarity	Vendor/brand	Ref.
1	Toluene (Tol.)	110	2.38	nonpolar	Sherwin Williams	48
2	Quinoline (Quin.)	237	8.98	nonpolar	TCI	49
3	Wash oil (Wash., USSteelWashOil, or USOil)	260	2.25	nonpolar		50
4	Carbon disulfide (CarbonDis.)	46	2.60	nonpolar		48

5	Benzene (Benz.)	80	2.27	nonpolar	Sigma-Aldrich	48
6	Ethanol (ETH)	78	24.50	polar		48
7	Pyridine	115	12.40	polar		48
8	Diesel	260	2.35	nonpolar		51
9	Benzene toluene xylene (BTX)	80	2.41	nonpolar		48
10	Blue Gem coal liquid (BGL)					

The following combinational liquids were studied for Carbores:

1. 25% quinoline and 75% toluene, designated as Quin.25%+Tol.75%
2. 50% quinoline and 50% toluene, designated as Quin.50%+Tol.50%
3. 50% quinoline and 50% US wash oil, designated as Quin.50%+USOil50%
4. 33% BGL, 33% BTX, and34% ethanol, designated as BGL33%+BTX33%+ETH34%

The following combinational liquids were studied for Koppers:

1. Quin.25%+Tol.75%
2. Quin.50%+Tol.50%
3. 50% carbon disulfide and 50% toluene, designated as CarbonDis.50%+Tol.50%
4. 33% wash oil, 33% BTX, and 34% ethanol, designated as Wash.33%+BTX33%+ETH34%

3.3.1.2 Mixture

The mixture for electrical separation tests of CTP comprised 20 g solid and 70 mL liquid. The mixture height was 25.4 mm below the top edge of the HV electrode when the large beaker was used.

For the candidate mixtures, at least one electrical test was conducted. Tests that showed promising deposit amounts, including the combinational tests, were followed by additional tests to confirm the repeatability of test results.

3.3.2 Solids for Modeling System

With the consideration in Section 2.1, several candidate solids were identified and examined in this study: sand, alumina, polyvinyl chloride (PVC), diatomaceous earth (DE), and zeolite. Details are listed in Table 7.

Table 7. Material condition of solids used modeling system for electrical separation study

Solid	Size (μm)	Density (g/cm^3)	Weight (g)	Solid volume (mL)	Solid volume (%)	Vendor/brand
Sand		1.52	2	1.32	1.9	—
Alumina	5	3.95	2	0.51	0.7	GNP Graystar (Douglasville, GA)
Polyvinyl chloride (PVC)	20	1.44	2	1.39	2.0	Georgia Gulf (Madison, MS)
Diatomaceous earth (DE)	100	2.25	2	0.89	1.3	Sigma-Aldrich, Celite 545
Zeolite Y, sodium		2.30	2	0.87	1.2	Thermo Scientific

3.3.2.1 Solvents

Two types of liquids were examined for modeling system study: toluene and mineral oil. Details are listed in Table 8.

Table 8. Candidate solvents for electrical tests on modeling system

Solvent	Density (g/cm^3)	Viscosity (mPa s)	Volume (mL)	Solid weight (g)	Solid weight (%)	Vendor/brand	Ref.
Toluene	0.865	0.59	70	60.55	3.3	Sherwin Williams	52
Mineral oil	0.855	107	70	59.85	3.3	Equate	53

3.3.2.2 Mixture

The mixture for tests of modeling systems comprised 2 g solid and 70 mL liquid. This composition corresponds to a mixture with 0.7–2.0 vol %, or 3.3 wt %, of solute.

3.4 EXPERIMENTAL PROCEDURE

The main procedures used in this study are illustrated in Figure 2. The procedure is briefly described in the following subsections.

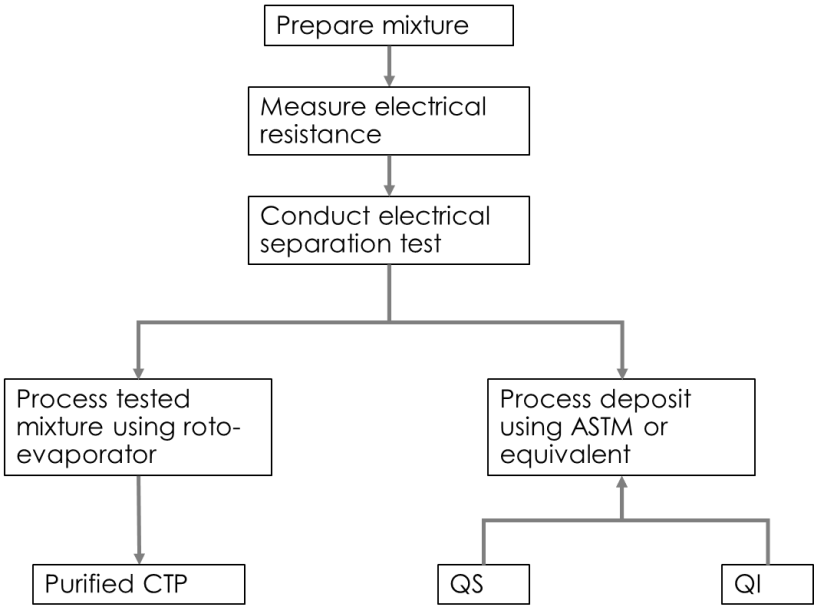

Figure 2. Flowchart of procedures for experimental study on coal tar pitch (CTP). QS: quinoline soluble; QI: quinoline insoluble.

3.4.1 Electrical Test

3.4.1.1 Preparation of Mixture and Setup

1. Add 20.0 g of pulverized CTP and 70 mL of solvent into a plastic bottle.
2. Shake the bottle to dissolve solid phase.

3. Check the electric resistance of the solution using an ohmmeter by holding measurement probes 1 in. (25.4 mm) apart. No electrical separation test will be pursued for the solution if the resistance is less than several megaohms.
4. Make the electrical connection of electrodes to HV and GRD cables.
5. Secure the plastic bracket to the beaker.
6. Pour the prepared solution into the beaker through the bracket openings.

3.4.1.2 Heating and Applying of Electrostatic Field

1. Start heating by using the hot plate's control button.
2. Stabilize the system at 35°C.
3. Enable the amplifier's HV capacity.
4. Start voltage generation by following a predetermined voltage profile.

3.4.1.3 Deposit Weight Measurement

1. Remove the deposit from the collecting electrode or the rod.
2. Dry the collected material under a hood at ambient conditions for at least 24 h.
3. Measure the weight.

3.4.2 EDS Analysis of Deposit

Material particles were collected for the selected tests from the area near electrode rod or disk and were mounted using conductive epoxy. A metallographic surface was prepared using a procedure developed for graphite samples. The metallographic samples were then analyzed using scanning electron microscopy (SEM) and X-ray energy dispersive spectroscopy (EDS).

3.4.3 Extraction and EDS Analysis of QI

To understand the composition of QI within the CTP and the deposit, QI extracts were obtained from the selected CTP and deposit by referring to ASTM procedure.[54]

As-ground CTP of 2 g and as-deposited materials were washed by using alternating quinoline and toluene and filtered using CFP1 filter paper four times. The extract was then dried in a vacuum oven at 115°C for 15 h until the variation of measured weight was within the specified range. The weights of extracted QI materials were used to evaluate the QI removal efficiency (RE).

The as-extracted QI materials from CTP and deposit were analyzed via SEM and EDS to confirm whether the QI of deposit had the same composition as that of the original CTP.

3.4.4 Analysis of QI-Removed Mixture

A roto-evaporator was used to further process the CTP mixture obtained by electrical separation. The current roto-evaporator has the following operating parameters:

1. Bath temperature: 90°C.
2. Condenser water temperature: 10°C.
3. Vacuum pressure: 41 mbar set point (normal operating range varies between 41 and 60 mbar).

Owing to the system's temperature capacity, the processing of CTP mixture was limited to the mixture of Carbores with toluene.

The extract from the roto-evaporator process can be used for the subsequent analysis to evaluate the effect of QI separation, including carbon fiber fabrication. The work in this report was limited to the measurement of softening points.

3.5 DATA PROCESSING

3.5.1 Electric Charge Estimate

The electric charge *Q* can be estimated according to signal *I* from the current monitoring channel of the HV amplifier by using Eq. (4):

$$Q = \int I\, dt, \tag{4}$$

3.5.2 Electric Energy Estimate

The electric energy E_E can be estimated according to voltage signal *V* and current signal *I* from monitoring channels of the HV amplifier by using Eq. (5):

$$E_E = \int V \cdot I\, dt, \tag{5}$$

3.5.3 Electric Field

The electric field inside the cylinder varies with the radial distance from the center. The averaged field level E_a was used in the evaluation and can be calculated using Eq. (6):

$$E_a = \frac{\int_a^b E(r)dr}{b-a} = \frac{V}{b-a}, \tag{6}$$

where *V* is the voltage applied to outer electrode, and *a* and *b* are the radii of the inner and outer electrodes, respectively.

3.5.4 Calculation of QI Removal Efficiency

The RE of QI can be estimated using Eq. (7):

$$\mathrm{RE} = \frac{W_2}{W_1} \times 100\%, \tag{7}$$

where W_1 is the weight of the original QI amount, and W_2 is the amount of QI that was removed.

4. EXPERIMENTAL RESULTS OF CTP

4.1 CONDITION OF MIXTURE AND OVERVIEW

4.1.1 Mixture Conductivity

A set of pictures are provided in Figure 3 to illustrate the condition of mixtures that were prepared for the electrical tests. The mixture with toluene as a solvent was generally heterogenous, as shown in test #64: Carbores mesh -80, toluene and in test #58: Carbores mesh -325, toluene. The undissolved particles are visibly attached to the inner wall of beaker.

The mixtures of quinoline and of ethanol were relatively homogenous and had a uniform dark color, as shown in test #53: Koppers mesh -80, Quin.50%+Tol.50% and in test #66: Koppers mesh -325, Wash33%+BTX33%+ETH34%.

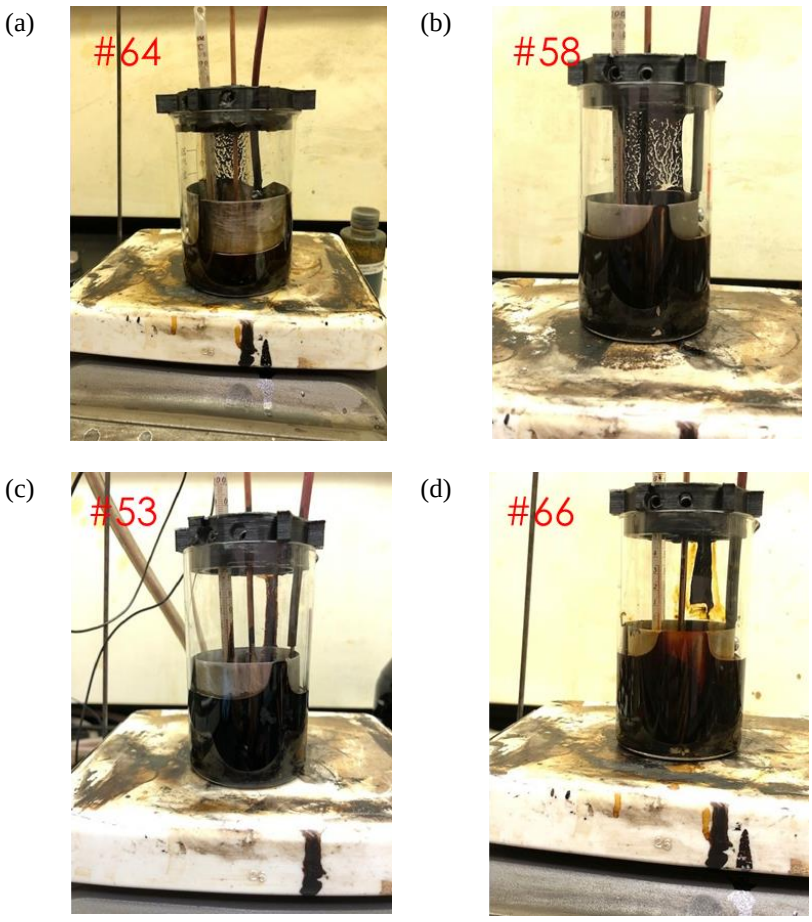

Figure 3. Heterogenous vs homogenous mixtures. (a) Carbores mesh -80, toluene, (b) Carbores mesh -325, toluene, (c) Koppoers mesh -80 Quin.50%+Tol.50%, (d) Koppers mesh -325 Wash33%+BTX33%+ETH34%

The electric resistance examination results are given in Table 9. The electric resistances of solutions with quinoline, ethanol, and pyridine were relatively low; therefore, these solutions were excluded from the electrical test. The solutions with toluene, wash oil, carbon disulfide, benzene, and diesel have been shown to be more electrically insulated, and the electrical tests of these solutions proceeded.

Table 9. Electric resistance of mixture at room temperature

Category	Solvents	Blue Gem	Springfield	Carbores	Koppers	Sand
I	Toluene (Tol.)	OC		OC	OC	
	Quinoline (Quin.)	0.5		SC	SC	
	Wash oil (Wash./ USSteelWashOil or USOil)	OC	OC	OC		OC
	Carbon disulfide (CarbonDis.)			OC	OC	
	Benzene (Benz.)			OC		
	Ethanol (ETH)			SC	SC	
	Pyridine			0.4		
	Diesel			OC		
II	CarbonDis.50%+Tol.50%				OC	
	Quin.50%+USOil50%			51		
	Quin.25%+Tol.75%				OC	
	Quin.50%+Tol.50%	0.8		[7, 24]	[7, 34]	
	Benz.71%+Tol.29%	6.2				
III	BGL33%+BTX33%+ETH34%			[5, 25]		
	Wash.33%+BTX33%+ETH34%				[10, 11]	

NOTE: OC: open circuit; SC: no resistance can be measured; number in the field indicates megaohms measured by voltmeter

The solution with quinoline cannot be used directly; hence, the combinational mixtures made of quinoline and toluene/carbon disulfide were explored. In these mixtures, the targeted QI can be separated more readily in solution by exploiting the solving capacity of quinoline. Simultaneously, the conductivity can be lowered by the high-resistance solvent. Usually, a solution of CTP with a mixed solvent can achieve a resistance of at least 5 MΩ. The same observation applies to the solution with the mixture of ethanol.

4.1.2 Overview of Electrical Separation Testing

Subsequent electrical tests were conducted on the mixtures that had acceptable electric resistance. The tests are summarized for all the tested CTPs (Cabores, Koppers, Blue Gem, and Springfield) in Table 10 through Table 13. The tests are listed in terms of category number (CN), series number (SN), test number (TN), solid, liquid, inner radius of outer electrode (IR_al [mm]), initial and maximum temperatures (TP1, TP2 [°C]), and deposit weight (g). The CN takes the form x_1-x_2, where

- x_1: I, II, III correspond to a liquid phase of one, two, or three parts, respectively, with nominal electrical setup (LB1/2 or SB1/2/3)
- x_1: IV denotes a reversed electrode (SB4)
- x_1: V denotes interrupted tests, bad electrical connections, or control tests
- x_2: 1, 2, 3 denote mesh 60/-80, -325, and tar of solid phase, respectively

The SN represents a combination of comprising liquid, mesh size of solid, and test condition. Each SN includes repeated tests if applicable.

Table 10. Summary of electrical test results with Carbores

CN	SN	TN	Solid (20 g)	Liquid (70 mL)	IR_al (mm)	TP1 (°C)	TP2 (°C)	Deposit (g)
I-1	1	35*	Carbores 60	Toluene	32.5	35	35	0.348
	1	37*	Carbores 60	Toluene	32.5	35	35	0.161
	2	39	Carbores 60	Toluene	32.5	35	35	0.579
	2	40	Carbores 60	Toluene	32.5	35	35	0.254
	3	42	Carbores -80	Toluene	27	35	35	3.760
	4	64	Carbores -80	Toluene	32.5	22	22	0.263
	5	59†	Carbores -80	Tol.100%	27	35	36	
	6	44	Carbores -80	USSteelWashOil	27	35	35	0.110
	7	62	Carbores -80	Bez.100%	27	35	35	0.099
I-2	8	58	Carbores -325	Toluene	27	35	35	3.100
	8	61	Carbores -325	Toluene	27	32	37	3.599
	8	77	Carbores -325	Toluene	27	35	37	2.901
	9	60	Carbores -325	CarbonDis.100%	27	35	37	1.341
II	10	47	Carbores -80	Quin.25%+Tol.75%	27	35	35	1.867
	10	68	Carbores -80	Quin.25%+Tol.75%	27	35	40	4.445
	10	74	Carbores -80	Quin.25%+Tol.75%	27	35	38	1.110
	10	79	Carbores -80	Quin.25%+Tol.75%	27	35	38	4.500
	11	55	Carbores -80	Quin.50%+USOil50%	27	35	47	1.023
	12	46	Carbores -80	Quin.50%+Tol.50%	27	35	58	2.603
	12	48	Carbores -80	Quin.50%+Tol.50%	27	35	50	3.881
	12	51	Carbores -80	Quin.50%+Tol.50%	27	35	53	2.390
	13	67	Carbores -80	Quin.50%+Tol.50%	27	23	28	
III	14	72	Carbores -80	BGL33%+BTX33%+ETH34%	27	35	47	8.031
	14	73	Carbores -80	BGL33%+BTX33%+ETH34%	27	35	48	1.880
	14	78	Carbores -80	BGL33%+BTX33%+ETH34%	27	35	45	6.202
IV	15	80	Carbores -80	Quin.50%+Tol.50%	27	35	75	4.125
	15	81	Carbores -80	Tol.100%	27	35	37	0.012
	15	82	Carbores -80	Quin.50%+Tol.50%	27	35	48	2.352
V	99	69	Carbores -80	Quin.50%+Tol.50%	27	35	110	0.901
	99	70	Carbores -80	Quin.50%+Tol.50%	27	35	95	0.447
	99	45a	Carbores -80	Pyridine				
	99	45b	Carbores -80	Diesel				
	99	47a‡	Carbores -80	Quin.50%+Tol.50%		35	35	
	99	59a‡	Carbores -80	Tol.100%		35	35	

* No modification on inner copper electrode

† Large disk attached to Cu rod, 3/4 in. (19.05 mm) diameter

‡ Control tests without field applied

Table 11. Summary of electrical test results with Koppers

CN	SN	TN	Solid (20 g)	Liquid (70 mL)	IR_al (mm)	TP1 (°C)	TP2 (°C)	Deposit (g)
I-1	1	38	Koppers 60	Toluene	32.5	35	35	0.168
	2	41	Koppers -80	Toluene	32.5	35	35	0.921
	3	43	Koppers -80	Toluene	27	35	35	1.968
II	4	57	Koppers -80	CarbonDis.50%+Tol.50%	27	35	38	4.687
	4	65	Koppers -80	CarbonDis.50%+Tol.50%	27	35	35	1.469
	4	93	Koppers -80	CarbonDis.50%+Tol.50%	27	35	36	5.103
I-1	5	56	Koppers -80	CarbonDis.100%	27	35	35	1.610
	5	76	Koppers -80	CarbonDis.100%	27	35	38	3.440
	5	92	Koppers -80	CarbonDis.100%	27	35	37	5.327
II	6	75	Koppers -80	Quin.25%+Tol.75%	27	32	40	3.171
	6	94	Koppers -80	Quin.25%+Tol.75%	27	35	40	6.501
	6	95	Koppers -80	Quin.25%+Tol.75%	27	35	40	8.611
	7	50	Koppers -80	Quin.50%+Tol.50%	27	35	46	4.020
	7	52	Koppers -80	Quin.50%+Tol.50%	27	35	57	3.597
	7	53	Koppers -80	Quin.50%+Tol.50%	27	35	49	2.412
	7	71	Koppers -80	Quin.50%+Tol.50%	27	35	46	0.712
III-2	8	63	Koppers -325	Wash.33%+BTX33%+ETH34%	27	20	41	4.217
	8	66	Koppers -325	Wash.33%+BTX33%+ETH34%	27	20	35	10.045
IV	9	54	Koppers -80	Quin.50%+Tol.50%	27	35	115	

Table 12. Summary of electrical test results with Blue Gem

CN	SN	TN	Solid (20 g)	Liquid (70 mL)	IR_al (mm)	TP1 (°C)	TP2 (°C)	Deposit (g)
I-3	1	34	BlueGem tar	WashOil	32.5	35	35	
I-1	2	36	BlueGem 60	Toluene	32.5	35	35	0.011
V	3	45	BlueGem -80	Quinoline	27	35	35	
	4	49	BlueGem -80	Benz.71%+Tol.29%	27	35	85	
	5	49a	BlueGem -80	Quin.50%+Tol.50%				

Table 13. Summary of electrical test results with Springfield

CN	SN	TN	Solid (20 g)	Liquid (70 mL)	IR_al (mm)	TP1 (°C)	TP2 (°C)	Deposit (g)
I-3	1	31	Springfield tar	WashOil	32.5	35	35	
	1	32	Springfield tar	WashOil	32.5	35	35	0.890

4.2 ELECTRICAL RESPONSES

4.2.1 Electric Current Response

4.2.1.1 Effect of solvents

Carbores

Electric current responses depend on the solvent, as shown in Figure 4 for Carbores. Among the solvents tested, the average level of electric current of solution increased in the following order: wash oil, benzene, toluene, carbon disulfide, Quin.25%+Tol.75%, Quin.50%+USOil50%, Quin.50%+Tol.50%, BGL33%+BTX33%+ETH34%. This order approximates the increase order of dielectric constant.

In general, the electric current closely followed the voltage profile, displaying a transient process in starting and ending stages, and a steady process in the constant voltage stage. The sustaining electric current signifies a constant charge movement existed, which probably constitutes the driving force for separation of solid particles. Decreasing current is obvious, especially for the high-level current process exhibited by Quin.50%+Tol.50%. The decrease in the electric current likely results from the consumption of existing electric charges.

The current response was consistent for a given composition of solution, as shown by the limited variation band for repeated tests.

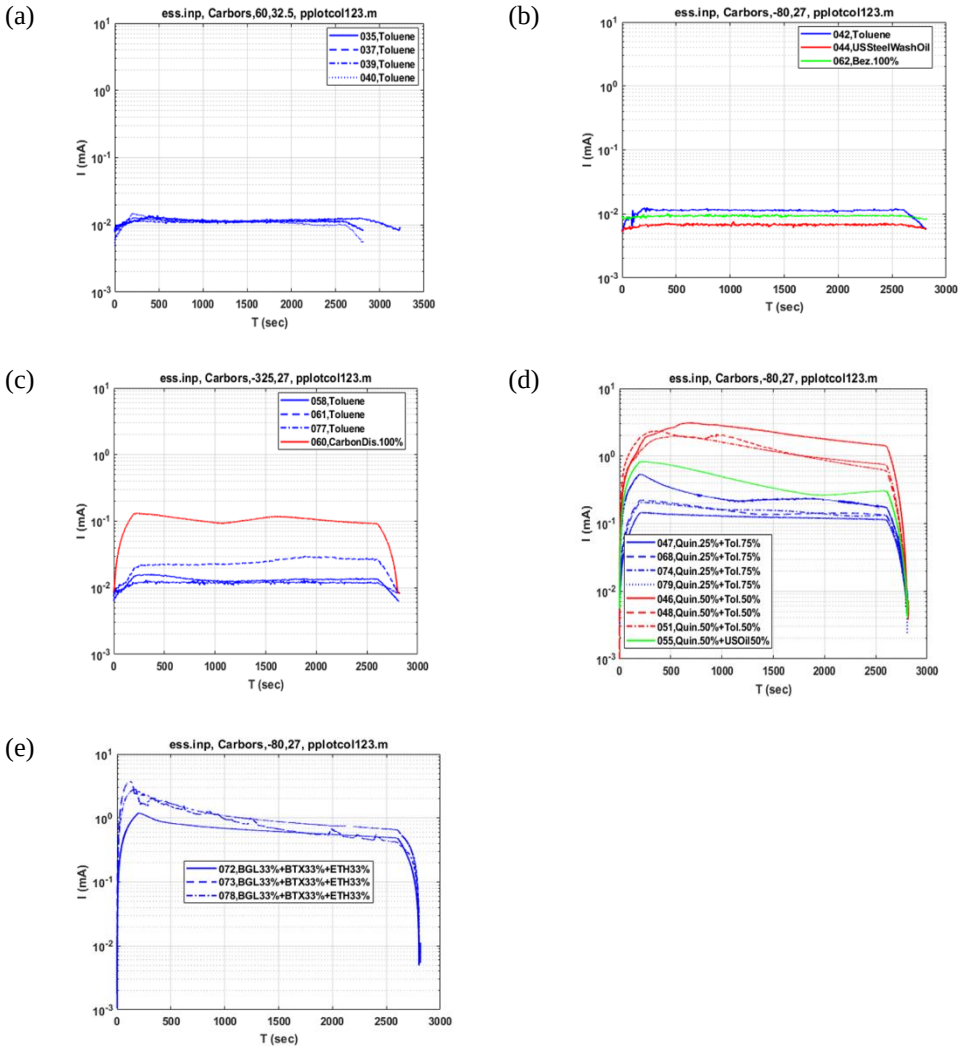

Figure 4. Electric current response of mixture of Cabrores. (a) Mesh 60 with toluene in beaker of radius 32.5 mm, (b) mesh -80 with toluene in beaker of radius 27 mm, (c) mesh -325 with carbon disulfide, (d) mesh -80 with quinoline composite liquids, (e) mesh -80 with ethanol composite liquid; mixture was heated to 35°C.

Koppers

The electric current in the case of Koppers (Figure 5) behaved similarly to that for Carbores. Among the tested solvents, the electric current increased in order as follows: toluene, CarbonDis.50%+Tol.50%, carbon disulfide, Quin.25%+Tol.75%, Quin.50%+Tol.50%, Wash.33%+BTX33%+ETH34%.

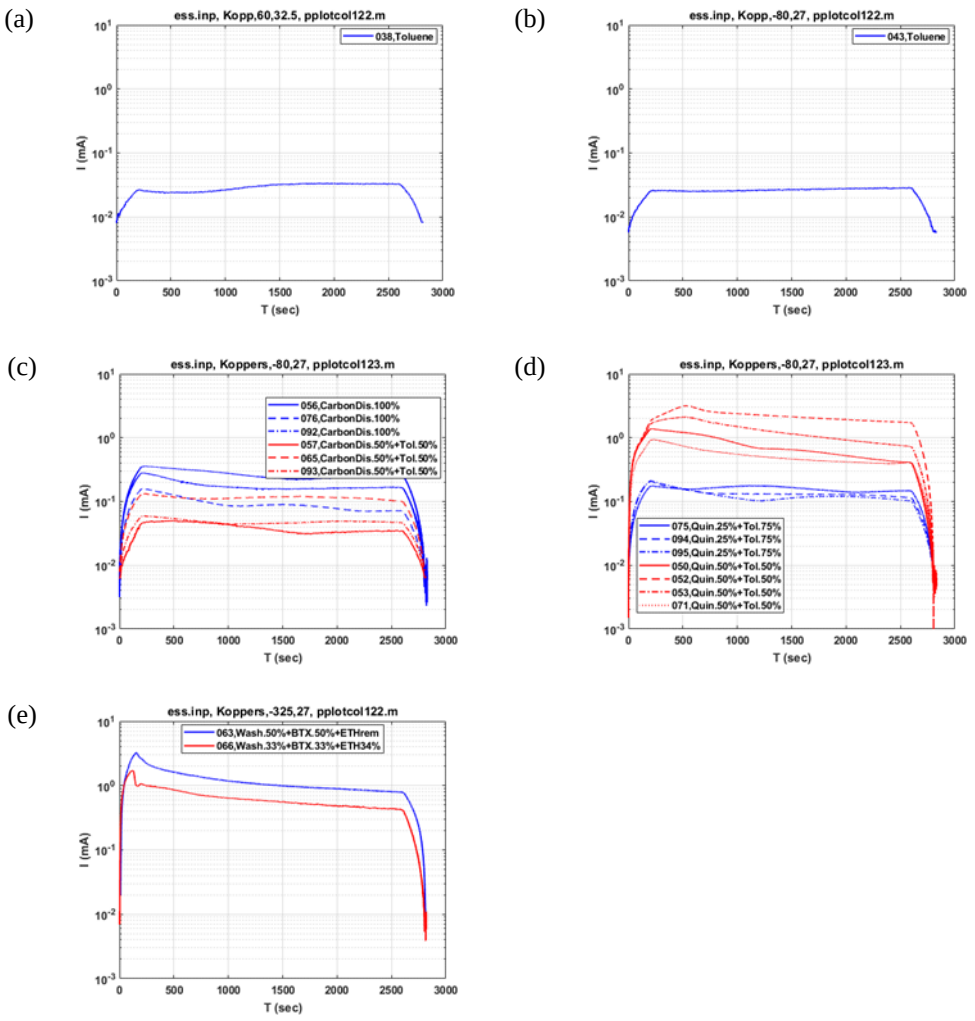

Figure 5. Electric current response of mixture of Koppers. (a) Mesh 60 with toluene in beaker of radius 32.5 mm, (b) mesh -80 with toluene in beaker of radius 27 mm, (c) mesh -80 with carbon disulfide, (d) mesh -80 with quinoline composite liquids, (e) mesh -80 with ethanol composite liquid. Mixtures were heated to 35°C.

In the toluene-only solvent, the current increased slightly. All the other solvents maintained a trend of decreasing current, as seen in Carbores.

The rate of decrease is especially profound for the Wash.33%+BTX33%+ETH34% solution.

4.2.1.2 Effect of solutes

The electric current curves of various solutes are grouped and illustrated in Figure 6. The results suggest that the electric current curves are only differential for the tests with toluene, but the difference is hardly seen in the cases of Quin.25%+Tol.75% and Quin.50%+Tol.50%.

Koppers and Blue Gem both appeared to be more kinetically active than Carbores in the toluene solvent, showing a higher level of current response. The high current response of Koppers seemingly corresponded to the low boiling point of this material, as discussed in the following subsections.

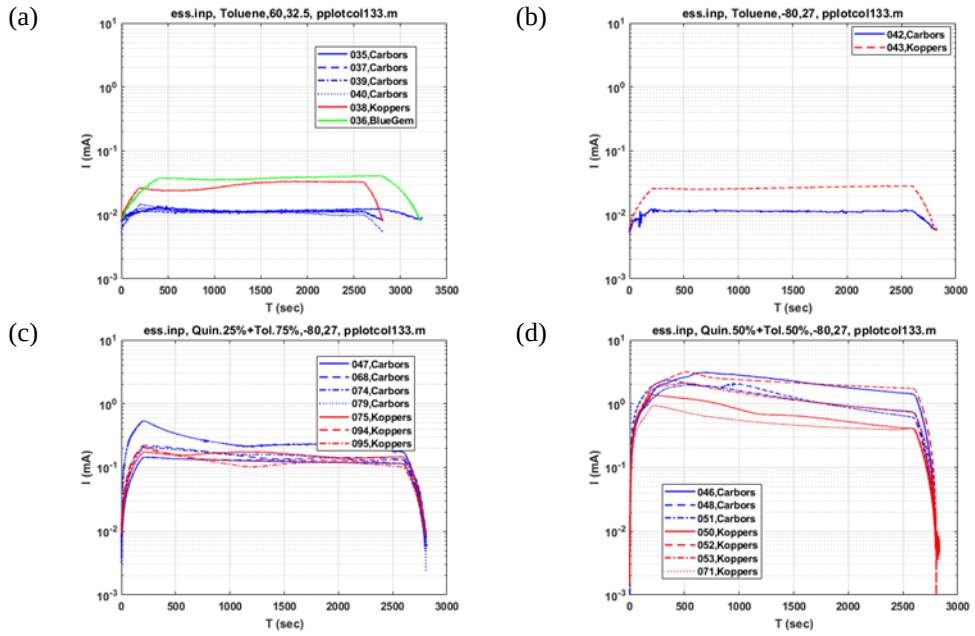

Figure 6. Electric current response of mixture of various solids. (a) Mesh 60 with toluene in beaker of radius 32.5 mm, (b) mesh -80 with toluene in beaker of radius 27 mm, (c, d) mesh -80 with quinoline composite liquids. Mixtures were heated to 35°C.

Solute mesh size

The powder with small size particles usually possesses more surface area of exposure to the attack from solvent. Thus, more charges or identities dissolved from CTP would be produced contributing to motion of charges. The high-level current was observed as expected in the case of Carbores with the mesh size was switched from -80 to -325, Figure 7 (b).

However, this was not the case for Koppers, Figure 7 (a), where the effect of mesh size was reverse for the reason unknown. It is understood that the test was limited for each mesh size, and the variation observed may be within the level of uncertainty for the condition tested.

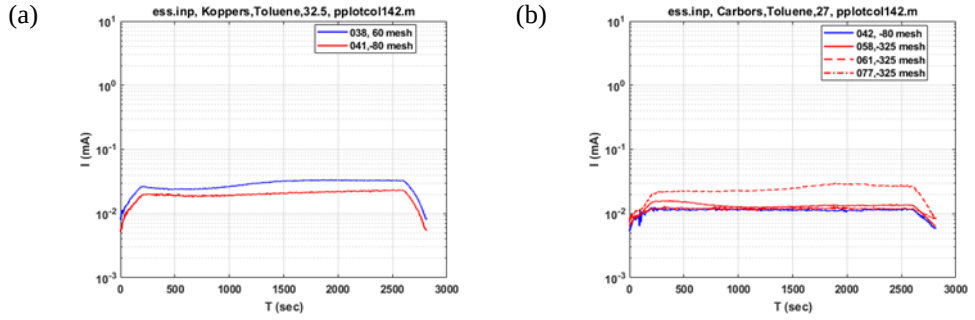

Figure 7. Electric current response of mixture. (a) Koppers with toluene in beaker of radius 32.5 mm, (b) Carbores with toluene in beaker of radius 27 mm. Mixtures were heated to 35°C.

4.2.1.3 Effect of electric field

Electric field level

The field level can be evaluated by varying the voltage applied for a given electrode configuration. To maximize the displacement and deposit, the field level effect was studied by using a specified voltage with different electrode spacings. As expected, a higher level of electric field produced a higher level of current response, as shown in Figure 8. High electric field is shown to enhance the electric current and deposit in both charge- and dipole-based scenarios.

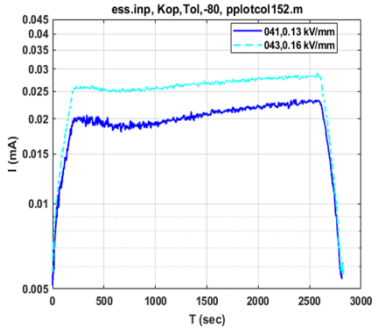

Figure 8. Electric current response of mixture for Koppers -80 mesh with toluene. Mixture was heated to 35°C.

Reversed electric field

With a voltage of 4 kV, the electric current increased rapidly when the copper rod served as an HV electrode and the aluminum cylinder as a GRD electrode. The tests were either paused or run with a lowered voltage to avoid tripping the amplifier. The surging of electric current signified a significant discharge occurring within the mixture. The relevant results are discussed in the following subsections.

4.2.2 Discussion

4.2.2.1 Electrical properties of mixture

CTP molecules are held by intermolecular bond forces such as dipole–dipole, dispersive, and hydrogen bonds. When mixed, the solvent destroys the intermolecular bond. The strong solvents such as quinoline, pyridine, and ethanol have been demonstrated to further break the covalent bonds of organic molecules. The lowered electric resistance of the as-prepared CTP mixtures using the strong solvents validate the existence of molecular ions. Heating introduces external energy into the system and improves dissolving. Depending on the temperature, covalent bonds can be broken, and the remaining molecular segment can become very active in chemical reaction, as explained by Zhu et al.[8]

The high electric field ionized the CTP molecules. Whereas the electrons resulting from the ionization are attracted to the positive (HV) electrode, the positive ions are repelled from it. These ions charge the undissolved and suspended particles. The positively charged particles are attracted to the GRD rod and are deposited. Thus, the positively charged particles recombine with the electrons from the outside circuit to close the loop.

The electric current is a comprehensive response of the space charges, mixture dielectric properties, and deposit's resistivity and permittivity. The ionized molecules can be quinoline or toluene soluble (QS or TS) or QI or toluene insoluble (TI). The number of molecular ions is apparently high when the amount of

strong solvent is high, corresponding to a high quantity of charging particles. These aspects obviously dominate the electric current response.

4.2.2.2 Stability of electrical separation

The setup in this study adopts the rod as GRD electrode, which is different from that of traditional wire–cylinder in ESP. No corona discharge or arcing were observed in the air above the mixture level, even though the electric field at the GRD is high compared with the HV electrode because of the electric field gradient.

With the same mixture, tests with a modified setup resulted in an abnormal response of electric current in several tests. The field reversed by using the rod as HV electrode and the cylinder as GRD electrode has a typical setup of ESP for positive corona. The rod apparently produced a higher electric field with a larger quantity of molecular ions than in a nominal setup condition, prompting a large electric current, as observed in the tests under condition SB4 (#54, #80). The tests appeared to be self-heating and experienced a considerable temperature increase during the test process.

The abrupt current increase indicates that a properly designed electrical setup is critical for an effective implementation of the ESS of CTP. A systematic electrical study is usually conducted to identify a safe area of operation. Obviously, such experimental work is also necessary for the laboratory study.

4.2.2.3 Main observations

- The current level of the solution of CTP–washing oil reported by Cao et al.[13] can be attained by using a mixture of quinoline and toluene for the CTPs examined in this study under same electrical load condition.
- The electric current tends to decrease during test period because of the decreasing quantity of charged particles.
- The reversed field corresponded to the configuration of ESP for positive corona discharge. The high electric field can result in a dielectric breakdown and lead to an abrupt current surge.

4.3 DEPOSIT RESPONSES

4.3.1 Deposit and Morphology

4.3.1.1 Carbores

Carbores was tested extensively with various solvents under different conditions in this study, and main experimental results of the deposit are presented in Table 10.

The deposit with the solvent that has a low dielectric constant was generally small, particularly for wash oil, toluene, and benzene. The mesh size imposed some effect on deposit, as shown by the results of mesh -325 with toluene. The carbon disulfide tended to produce a high yield. However, the multipart solvents with carbon disulfide, quinoline, and ethanol usually exhibited a sizable deposit of several grams, which was about one order of magnitude more than those of single-part solvents for mesh 60 and -80 solutes.

The deposit exhibited a large variety of geometrical shapes, as shown in Figure 9 through Figure 12, according to the solvents used in the categories. Observed shapes were a cylinder with expanded head (#39), cone (#62, 68, 55), cup (#58, 60, 47), rock candy (#46), hat (#48), and thickened disk (#72).

(a) 

(b) 

Figure 9. Geometrical shape of deposits with Carbores. (a) #39: mesh 60, toluene, 32.5 mm; (b) #62: mesh -80, 100% benzene, 27 mm.

(a) 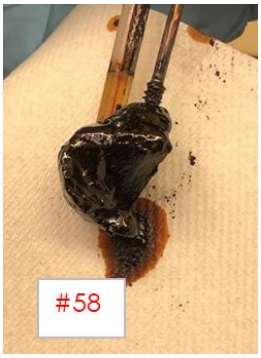

(b) 

Figure 10. Geometrical shape of deposits with Carbores. (a) #58: mesh -325, toluene, 27 mm; (b) #60: mesh -325, carbon disulfide, 27 mm.

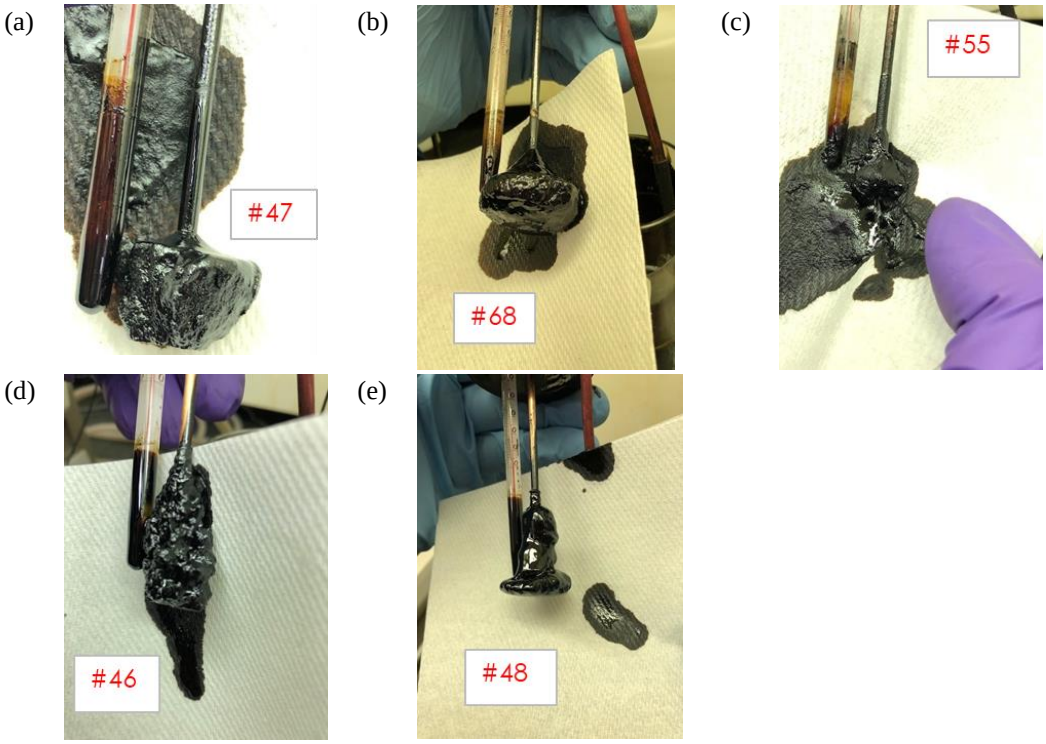

Figure 11. Geometrical shape of deposits with Carbores. (a, b) #47, 68: mesh -80, Quin.25%+Tol.75%, 27 mm; (c) #55: mesh -80, Quin.50%+USOil50%, 27 mm; (d, e) #46, 48: mesh -80, Quin.50%+Tol.50%, 27 mm.

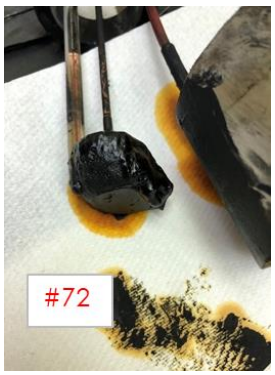

Figure 12. Geometrical shape of deposits with Carbores. #72: mesh -80, BGL33%+BTX33%+ETH34%, 27 mm.

A quantitative characterization of the deposit is beyond the scope of this study. The final geometrical shape and size of deposit displayed represent a comprehensive result of factors; for example, electric force, drag or thermal diffusion, and gravitation. The pull of the rod electrode from the beaker also had some effect on the deposit obtained.

The deposit body was generally composed of a soft surface layer and a solidified core. The soft layer can be removed manually with tissue paper, whereas the core may be hardened and requires a tool to scrap off the electrode, especially for those of two-part solvents with quinoline.

In addition to the deposit around the electrode, a viscous layer of sediment was usually present on the bottom of the beaker. The layer of sediment can be seen from the side surface of the deposit; for example, test #39, 58, and 60. The part of sediment may be from the electrical test process but dropped when the rod was pulled out because the rod could not hold it.

A slurry was observed on the bottom of the beaker after tests with most of the examined mixtures, especially mesh -325 in both toluene and carbon disulfide, and mesh -80 with the three-part solvent with ethanol. For tests with a two-part solvent with quinoline, the bottom of the beaker looked clean without significant slurry.

4.3.1.2 Koppers

The deposit response of Koppers mixture was similar to that of Carbores; the experimental results and the test conditions and categories are given in Table 11. Particularly, the deposit with the single-part toluene solvent is smaller than multipart solvents. The corresponding deposit weight exhibited a wide range of variation, usually several grams; for example, it varied from 1.610 g to 5.327 g for carbon disulfide. The range of variation was even larger for the Wash.33%+BTX33%+ETH34% solvent.

The deposit morphology varied as, shown in Figure 13 through Figure 15, and included thickened disks (#38, 41), cones (#95, 50, 43), rock candy (#56), and cups (#57, 94, 66).

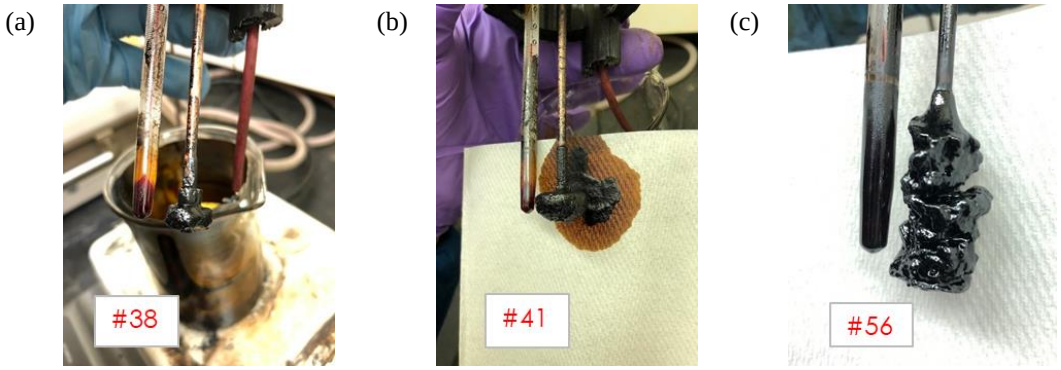

Figure 13. Geometrical shape of deposits with Koppers. (a) #38: mesh 60, toluene, 32.5 mm; (b) #41: mesh -80, toluene, 32.5 mm; (c) #56: mesh -80, carbon disulfide, 27 mm.

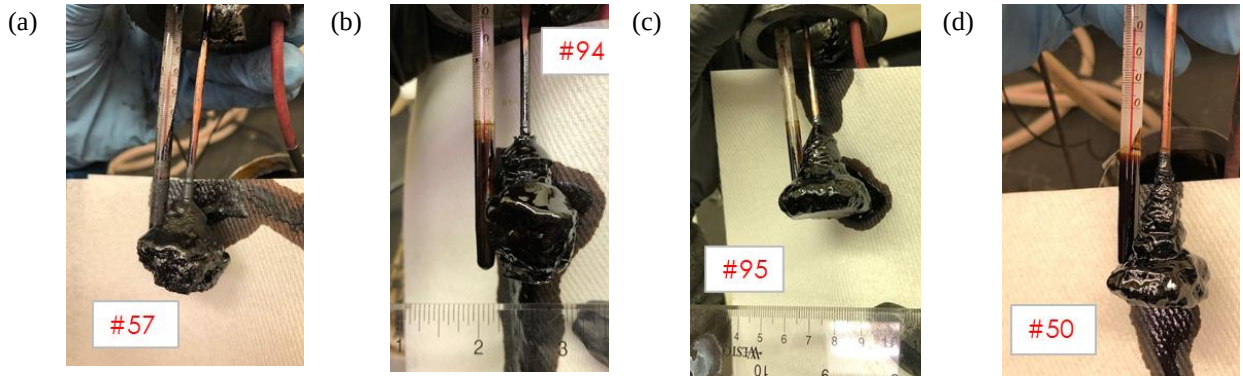

Figure 14 Geometrical shape of deposits with Koppers. (a) #57: mesh -80, CarDis.50%+Tol.50%, 27 mm; (b, c) #94, 95: mesh -80, Quin.25%+Tol.75%, 27 mm; (d) #50: mesh -80, Quin.50%+Tol.50%, 27 mm.

(a) 

(b) 

Figure 15. Geometrical shape of deposits with Koppers. (a) #63: mesh -325, Wash.33%+BTX33%+ETH34%, 27 mm, (b) #66: mesh -325, Wash.33%+BTX33%+ETH34%, 27 mm.

Again, an appreciable amount of slurry was present on the bottom of the beaker for tests with carbon sulfide and its mixture with toluene.

The deposits with carbon disulfide and the two-part solvents of quinoline and of carbon disulfide featured a densified core.

4.3.1.3 Blue Gem

Effort was made to test Blue Gem for both tar and mesh sizes 60 and -80. The yield for the one with toluene as solvent was obtained but relatively low, as shown in Table 12. No image of a deposit is available for this test. The tests using quinoline and two-part solvents of benzene and quinoline could not be conducted because the electric resistance of the mixture was too low.

4.3.1.4 Springfield

Two runs were performed for Springfield tar using washing oil (Table 13). As shown in Figure 16, the deposit assumed a conical shape for the electrical test with a deposit weight of 0.890 g.

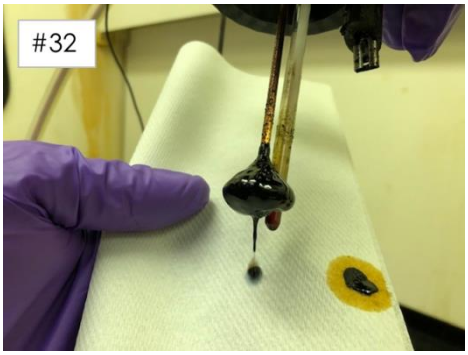

Figure 16. Geometrical shape of deposits with Springfield. #32: tar, washing oil, 32.5 mm.

4.3.1.5 Reversed Field

Carbores mesh -80 with Quin.50%+Tol. 50%

A mixture of Carbores mesh -80 with Quin.50%+Tol. 50% solvent was tested with electrodes switched (TN #80) (i.e., the electric field directed outward). The mixture exhibited a very fast current increase, which required reducing the electric field level to prevent the potential circuit trip, as shown in Figure 17.

(a) (b) (c)

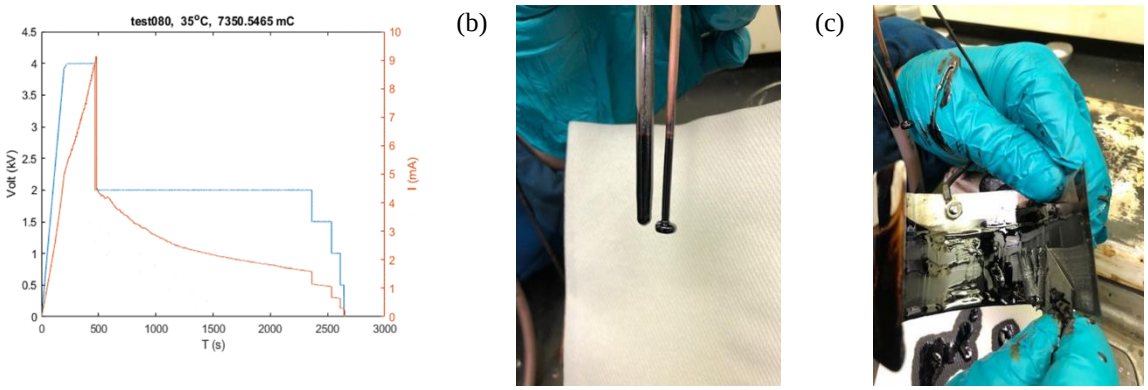

Figure 17. Carbores mesh -80 (20 g) in 70 mL Quin.50%+Tol.50%. (a) Electric current response, (b) TN #80, no deposit on HV copper rod, and (c) TN #80, deposit GRD aluminum sheet. Homogenous solution, self-heat; hard layer deposit on sheet; clean bottom; 35°C.

A multilayer structure was deposited on the aluminum sheet. The top layer was shining and soft, and the bottom layer was hard. A razor was used to remove the deposit. The weight of dried deposit was measured as 4.125 g, which is more than the deposits (TN# 46, 48, 51) obtained with the same mixture in the nominal electric field setup. However, no deposit was observed on the center copper rod.

An additional test (TN #82) was performed for the same mixture but with a lower voltage (2 kV) to obtain a complete test with constant voltage. As before, no appreciable deposit was observed on the copper rod; a thin layer of deposit was produced on the aluminum sheet (not shown), and the weight of deposit was 2.352 g.

Carbores mesh -80 with toluene

TN #81 was also conducted under the reversed field with Carbores mesh -80 and toluene. The responses are presented in Figure 18.

(a) (b) (c)

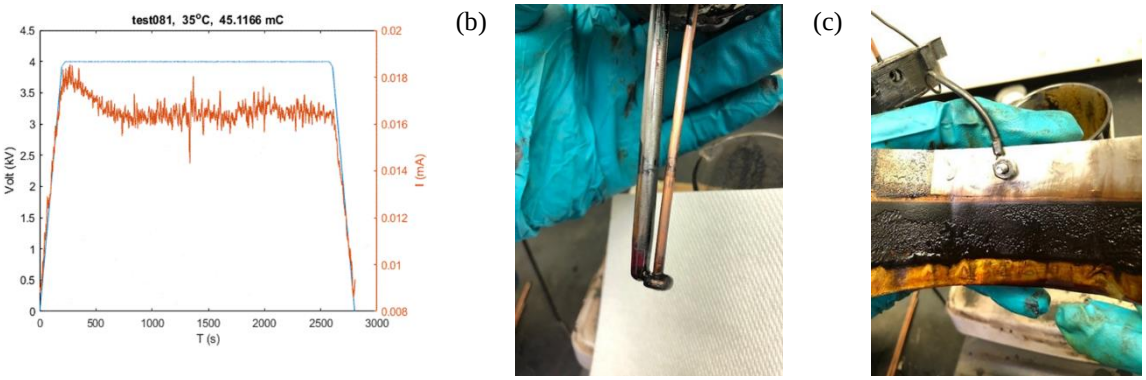

Figure 18. Carbores mesh -80 (20 g) in 70 mL toluene. (a) Electric current response, (b) no deposit of TN #81 on HV copper rod, and (c) deposit of TN #81 on GRD aluminum sheet. Homogenous solution, self-heat, soft deposit on sheet, bottom had hard sediment; 35°C.

Again, no deposit was observed on the center copper rod. A thin layer developed on the surface of the aluminum sheet with a coarse surface. The bond between coating and substrate appeared to be quite strong, and a tool was required to remove it. The deposit was weighed about 0.012 g after dried, which is less than that obtained for the same mixture in the nominal setup (TN #42).

4.3.2 Deposit Weight

4.3.2.1 Solvent effects

The material deposit weight responses are presented as a function of solvents, as shown in Figure 19. The data are pooled for a solute with various mesh sizes; for example, the bar for Carbores includes meshes 60, -80, and -325.

(a) (b)

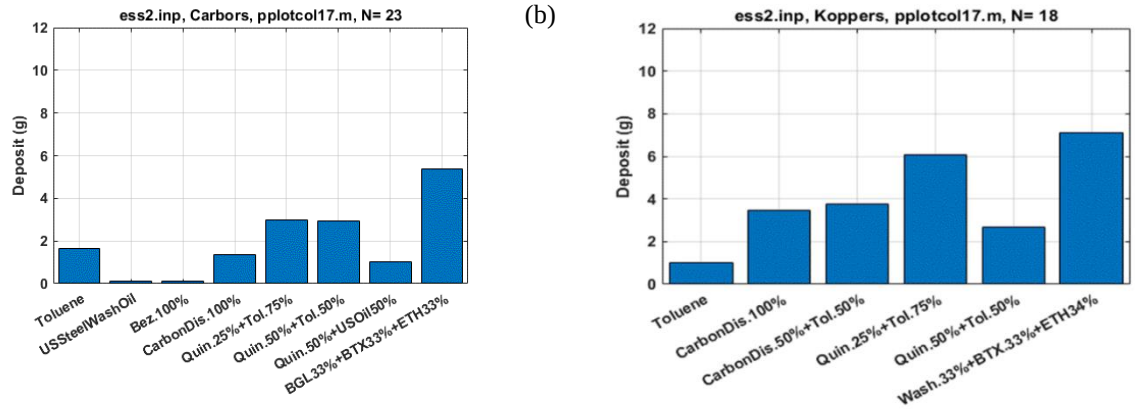

Figure 19. Deposit response of mixtures with various solvents. (a) Carbores and (b) Koppers. Test temperature 35°C.

In the case of Carbores, the deposits with toluene and carbon disulfide solvents were the highest among single-part solvents. Two- and three-part solvents with quinoline and ethanol generated more deposit than single-part solvents. Similar observations hold for deposits with Koppers.

4.3.2.2 Effect of solutes

The deposit response as a function of solute is shown in Figure 20. For toluene, Blue Gem had a relatively low yield. However, such observation cannot be over-emphasized because of the small number of data points.

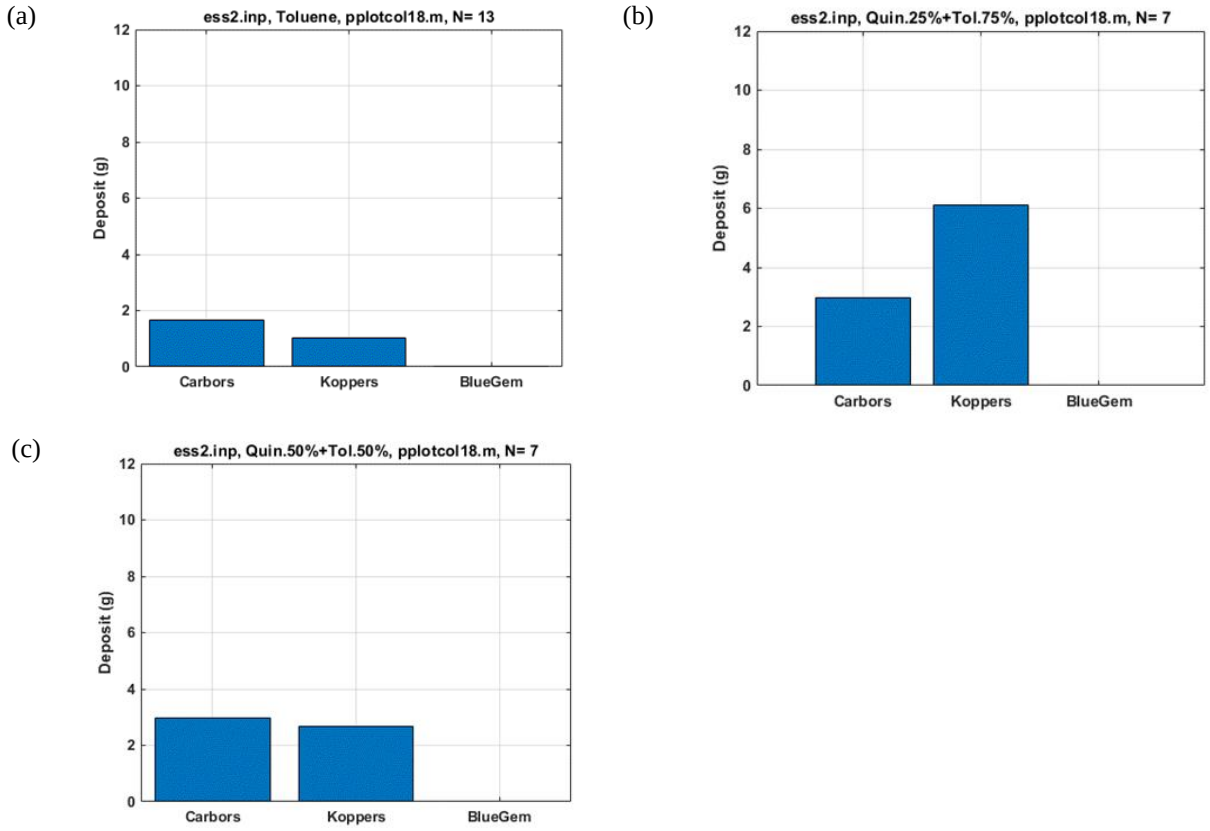

Figure 20. Deposit weight response as a function of solutes for various solvents. (a) Toluene, (b) Quin.25%+Tol.75%, and (c) Quin.50%+Tol.50%.

For two-part solvents with quinoline, electrical separation can produce a more sizable deposit for Koppers than for Carbores in the case of the Quin.25%+Tol.75% solvent. The trend was reversed for Quin.50%+Tol.50%, but the difference is insignificant.

4.3.2.3 Effect of electric field

The summary for Carbores (Table 10) shows that the weight of deposit obtained using the high-field setup SB2 (TN #42) was higher than those for the lower field setup LB2 (TN #39, 40), disregarding mesh size difference of solute. Furthermore, the weight of deposit obtained using the reversed field for the same mixture was higher than but still near the range of test results with a nominal field.

However, no conclusions can be made because the number of data points was limited or the test voltage in the case of the reversed electric field was not maintained constant as in the nominal condition.

4.3.2.4 Correlation to electrical response

Carbores

Figure 21 presents the deposit of Carbores as a function of electric charge and electric energy. The tests of various solvents for the given solute covered a range of electric charges of several orders of magnitude. A relation exists between the material deposit and electric charge, even though the data points are widely scattered owing to the variation of test conditions. The deposit exhibited a high increase rate in the range of less than 100 mC, after which the increase rate slowed.

(a)

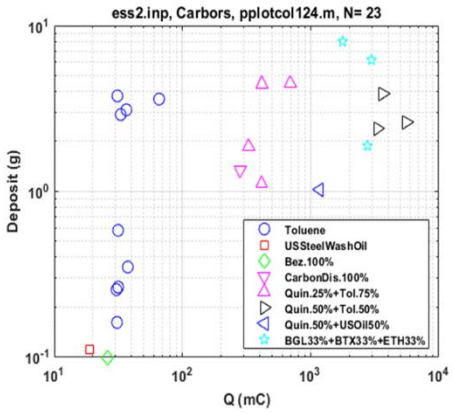

(b)

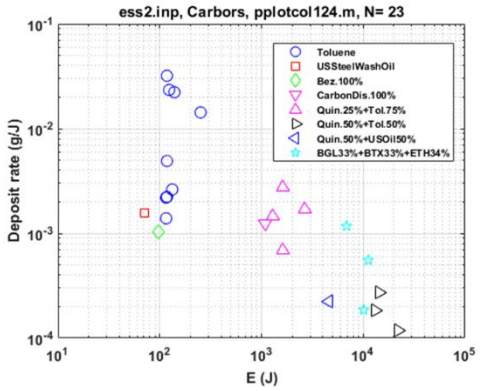

Figure 21. Carbores deposit as a function of electric charge and energy. (a) Correlation of deposit weight to accumulated charge and (b) unit deposit for Carbores with various solvents.

Furthermore, the unit deposit weight with respect to electrical energy decreases with increasing electric charge, as expected. In the case of Carbores, the greatest energy consumed occurred for Quin.50%+Tol.50%; the second greatest energy consumed occurred for BGL33%+BTX33%+ETH34%. Therefore, an optimized solvent for the electrical separation of subject solute must consider both the weight production and the energy consumption.

Koppers

The deposit response of Koppers is given in Figure 22. The greatest deposit weights occurred with carbon disulfide, Quin.25%+Tol.75%, and CarbonDis.50%+Tol.50%. Moreover, the electrical separation with Quin.50%+Tol.50% consumed the highest energy among all the solvents tested.

(a)

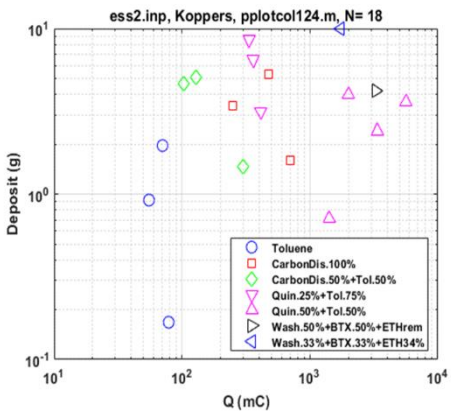

(b)

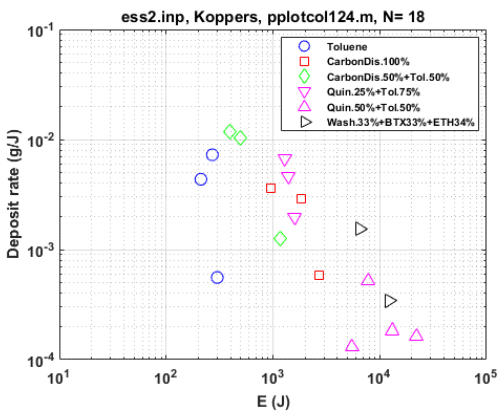

Figure 22. Koppers deposit as a function of electric charge and energy. (a) Correlation of deposit weight to accumulated charge and (b) unit deposit for Koppers with various solvents.

Pooled data

The relation of deposit weight to electric charges can be approximated by using a linear equation on a double log plot as follows:

$$y = p_1 x + p_2, \tag{8}$$

where $x = \ln(Q)$, $y = \ln(w)$, Q is the electric charge (mC), and w is the deposit weight (g). The data points for Carbores and Koppers were pooled to increase the confidence level of the estimate, and the curve fitting resulted in $p_1 = 0.387$ and $p_2 = -1.632$, as shown in Figure 23.

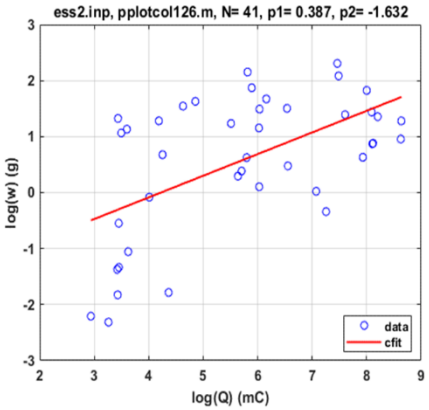

Figure 23. Correlation of deposit weight to accumulated charge for Carbores and Koppers mixtures with various solvents.

4.3.3 Discussion

4.3.3.1 Electromechanical behavior of particles

The deposit formed represents a comprehensive electromechanical response of a mixture, especially of solids. The solid and the electric field exhibit a coupling in which the electric field drives the solid and the solid's motion compromises the evolution of space charges and the alternation of the collecting electrode.

Effective gravitational force

In addition to the electric force, the solid particle also experiences other forces, noticeably including gravity and drag. The effective gravitational force, F_G, can be written as

$$F_G = \frac{4}{3}\pi {r_p}^3(\rho_p - \rho_f)g, \quad (9)$$

where r_p is the particle radius, ρ_p is the particle density, ρ_f is the liquid density, and g is the gravitational acceleration. The particle tends to settle if the buoyancy cannot offset the gravity, and the electric force cannot drive it fast enough to the collect electrode. The sizable slurry observed on the bottom of beaker indicates a significant contribution of gravitational force that existed and induced settling of particles in the cases of a single-part solvent and of multipart solvents that include carbon disulfide and ethanol.

The fluid flow was introduced and studied previously to slow the settlement of particles in the electric field; for example, in Pohl,[27] Benguigui and Lin,[33] and Li et al.[39] The flow rate was used to control the effect of gravity and ensure the effectively imposed electric field action. A pump or pressure source was incorporated into the ESS to generate the flow. This option should be considered to improve control of the particle motion in CTP mixture.

Viscous force

According to the Stokes equation, the viscous or drag force, F_D, on a particle can be written as follows:

$$F_D = -6\pi\eta r_p(u_p - u_f), \quad (10)$$

where η is the dynamic viscosity of the fluid, r_p is the particle radius, u_p is the particle velocity, and u_f is the fluid velocity. A well-characterized viscosity of mixture is critical for the effective transport of a particle in the electric field. The viscosity of mixture depends on the liquid phase and the mixture ratio. The effect of viscosity was not evaluated in this study but can be seen from the electrical testing of the modeling system, as discussed in Section 5.

In many cases, the identification of solvents for ESS must take account of viscosity from the beginning. Heating and flow rate can also be used in the ESS operation to tune the viscosity of fluid and facilitate the deposit.

Reversed field setup

Reversing the electrical direction from inward to outward changed the deposit direction for all the conditions tested. This fact signifies that the electric force that governs particle motion is charge based. The direction of deposit would be same if the particle's motion were governed by dipole-based electric force, as elaborated by Pohl,[27, 29] which was apparently not the case in the present study.

The understanding of deposit mechanism developed here thus validates the electrical responses observed as described in Section 4.2, in which the conductivity of mixture and electric displacement originated from the response of molecular ions; that is, the positively charged particles ultimately fueled the deposit as observed.

4.3.3.2 Main observations

- Deposit of particles in CTP mixture can be effectively implemented in a wire–cylinder configuration, as proposed and examined this study.
- Deposit depends on the solvents. Various types of the candidate solvents were examined, including single-part and multipart solvents. Among the solvents tested, two-part and three-part solvents containing quinoline and ethanol produced the highest deposit weight.
- For the CTPs tested, the deposit depended on the type of CTPs less than on the solvents used.
- The deposit process examined in this study is originated from the charged particles. An appreciable relation exists between deposit weight and electric charge.

4.4 QI AND PROCESSED CTP

4.4.1 QI Estimates

4.4.1.1 As-Received CTP

Processing the Carbores mesh -80 and Koppers mesh -80 using the procedure described in Section 3.4 resulted in QI ratios of 14.176% and 10.629%, respectively (Table 14).

Table 14. QI extracts of as-prepared CTP

Solid	Starting weight (g)	Ending weight (QI, g)	QI weight ratio (%)
Carbores -80	2.056	0.292	14.176
Koppers -80	2.094	0.197	10.629

4.4.1.2 Deposit

QI particles were also extracted from deposits by using the procedure also outlined in Section 3.4 for the selected tests: TN #58, 48, 53, and 65 (Table 15). The weight ratio of QI particles to deposit attained the highest level with Quin.50%+Tol.50%, about 54% to 56%. For toluene and CarDis.50%+Tol.50%, the weight ratio was around 32%.

Table 15 QI Extract of Deposit

TN	Solid	Liquid	Deposit (g)	Extract (QI, g)	Ratio (%)	RE (%)
#58	Carbores -325	Tol.100%	3.100	1.001	32.29	35.3
#48	Carbores -80	Quin.50%+Tol.50%	3.881	2.160	55.66	76.2
#53	Koppers -80	Quin.50%+Tol.50%	2.412	1.310	54.31	61.6
#65	Koppers -80	CarDis.50%+Tol.50%	1.469	0.477	32.47	22.4

The content of QI particles in a deposit can be related to the physical condition of deposit. The deposit with Quin.50%+Tol.50% was usually densified because it contained more QI particles. On the other hand, most of the deposit of Carbores mesh -325 was loosely bonded because it contained more QS particles, about 68%. The QI ratios obtained in this study are higher than those in the CTP evaluated by Cao et al.,[13] as illustrated in Figure 24..

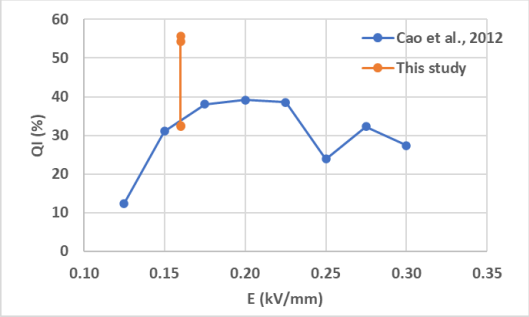

Figure 24. Weight ratio of QI to deposit. Temperature 35°C, 40 min.

4.4.1.3 QI Removal Efficiency

The QI RE was estimated using information on QI ratio of the CTP in Table 14 and is listed in the last column of Table 15. The RE of QI depends on the solvent. Among the examined cases, Quin.50%+Tol.50% offers the highest level of RE; it reached as high as 76.2% for Carbores and 61.6% for Koppers.

Improved RE is possible. Cao et al. reported an RE of 100% using washing oil as a solvent on the CTP they studied under an electrical level of 0.23 kV/mm. The RE had a monotonic increase before that field.[13] Therefore, the RE can be increased if the field level increases from 0.16 kV/mm that was used in this study to 0.23 kV/mm, as shown in Figure 25.

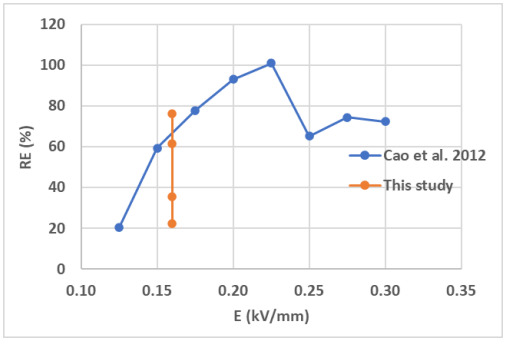

Figure 25. Removal efficiency of QI as a function of electric field. Temperature 35°C, 40 min.

4.4.2 Processed CTP

A roto-evaporator was used to process the QI-removed CTP mixture, as discussed in Section 3.4. The extraction of the Carbores mixture with toluene resulted in a product of 14.73 g, as shown in Figure 26 for TN #42. Considering the deposit was about 3.76 g, the total recovered was about 18.49 g, which is less than the material input of 20 g. Apparently, material loss occurred with the various procedures.

(a)  (b) 

Figure 26. Processed CTP. (a) Mixture after electric test and collected deposit; (b) extracted pitch product, 14.73 g; #42 Carbores -80 mesh, toluene 100%, 0.16 kV/mm.

The softening point (SP) of pitch increased after the QI particles were removed, as shown in Table 16. For Carbores, the increase was about 40% and for Koppers about 23%. The increase in SP reflects the effect of QI removal on the performance of pitch.

Table 16. Softening point of pitch increased after QI particles were removed

TN	CTP	Solvent	Initial SP (°C)	Final SP (°C)	Increase ratio (%)
#39	Carbores 60	Toluene	200	280	40
#42	Carbores -80	Toluene	200	280	40
#41	Koppers -80	Toluene	110	135	23

4.4.3 Discussion

4.4.3.1 QI ratio of deposit

Some of the QS molecules were apparently pulled into the collecting rod along with the QI particles during the electrical separation. For the samples analyzed, QI particles made up 32% to 56% of the deposit.

The further removal of the QI particles from the deposit requires a secondary separation process. Whether the non-QI material is recovered relies on the composition and the technoeconomic analysis of the process involved.

4.4.3.2 RE of QI and electric energy

The RE of QI particles strongly depends on the solvent. For a given CTP, the solvent likely must be customized and designed for an effective ESS. As mentioned previously, the two-part mixture of quinoline achieved the highest RE, 67%–77%, with the setup capacity up to 0.16 kV/mm.

Furthermore, the electric energy for these solvents varied. For the solvents that could generate several grams of the deposit (toluene, carbon disulfide, two-part and three-part mixtures), the electric energy was within a range of from 1.0×10^3 to 2.0×10^4 J (Figure 21, Figure 22). A field level of 0.23 kV/mm—about 1.438 times the field used in the current study—is likely required to achieve a full removal of QI material.

If a constant electric resistance is assumed, then the energy consumed can be increased to 2×10^3 to 4×10^4 J for 100% RE in the ESS. Generally, the electric resistance increases, and the energy would be lower than the estimate. Cao et al. reported the energy consumption of the centrifugal method for the QI separation of CTP mixture could reach as high as 1.1×10^5 J.[13] Therefore, a good opportunity exists to reduce the energy consumed.

4.4.3.3 Main observations

- The RE of ESS process can reach as high as 76.2% for Carbores and 61.6% for Koppers.
- The RE can be further enhanced if the field level increases from 0.16 kV/mm that was used in the current study to 0.23 kV/mm, according to the relation established between the RE and the electric field.

5. EXPERIMENTAL RESULTS OF MODELING SYSTEM

Not all the tests exhibit the expected visible pattern. The deposit apparently depended on the properties of solid and liquid phases. The density and viscosity were found to play a critical role in demonstrating the mechanism of ESS in a model system. For the mixture of sand and alumina with mineral oil, neither deposit nor pattern was observed. However, the mixtures of PVC, DE, and zeolite exhibited either deposit or driving pattern. The following discussion focuses on the results of PVC and DE. The electrical test conditions and results are summarized in Table 17 and Table 18 for the two modeling systems.

Table 17. Summary of electrical test results with PVC model system

CN	SN	TN	Solid (2 g)	Liquid (70 mL)	IR_al (mm)	TP1 (°C)	TP2 (°C)	Deposit
I	1	83	PVC 20 μm	Toluene	27	35	35	Suspension with fine particles; rod clean, deposit particles on edge of sheet/bottom; inward field
	2	87	PVC 20 μm	Mineral oil	27	35	54	Fine particle suspension with a milky appearance, rod/ sheet clean; no pattern showed up under electric field; inward field
IV	3	90*	PVC 20 μm	Toluene	27	35	35	Deposit on rod; 0.8 mm pileup in center of sediment; reversed or outward field

* 20 mins used for 4 kV

Table 18. Summary of electrical test results with DE model system

CN	SN	TN	Solid (2 g)	Liquid (70 mL)	IR_al (mm)	TP1 (°C)	TP2 (°C)	Deposit
I	1	84	DE 100 μm	Mineral oil	27	35	43	Rod/sheet clean, 0.97 mm thicker sediment in center; inward field
	2	85	DE 100 μm*	Mineral oil	27	35	43	Rod/sheet clean; diluted mixture did not show any sign of pattern caused by electric field or deposit; inward field
IV	3	88†	DE 100 μm	Mineral oil	27	22	22	Rod/sheet clean; no pattern observed; reversed or outward field
	4	89†	DE 100 μm	Mineral oil	27	35	38	Rod/sheet clean, 3 mm thicker sediment around sheet; outward field

* 0.25 g of solid used
† 20 mins used for 4 kV

5.1 PVC

5.1.1 Inward Electric Field

The mixture of 2 g PVC and 70 mL toluene appeared to be a typical suspension with fine particles visible. The model system responded with electric current similarly to that of a mixture of Carbores mesh -80 with toluene, as shown for TN #83 in Figure 27.

(a) (b) (c)

Figure 27. TN #83: 2 g PVC in 70 mL toluene. (a) Electric current response, (b) mixture at 10 min, showing several diverging traces developed on bottom, and (c) deposit on the lower edge of aluminum sheet. Rod as GRD electrode, sheet as HV electrode; suspension with fine particles; 35°C.

Several diverging traces developed on the bottom of the beaker 10 min after the voltage profile started. The dark color is that of the hot plate's top surface. The deposit accumulated on the lower edge of the aluminum sheet, but the copper rod was clean. Thus, the particle was driven by the negatively charged particles that moved against the electric field and produced the deposit on the outer electrode.

5.1.2 Outward Electric Field

An additional test, TN #90, was conducted using the PVC mixture composed of 2 g PVC powder and 70 mL toluene at 35°C but with the electric field direction reversed (i.e., the copper rod was the HV electrode, and the aluminum sheet was the GRD electrode). As shown in Figure 28, the electric current responded with a falling curve during the process; this trend is similar to TN #83.

(a)

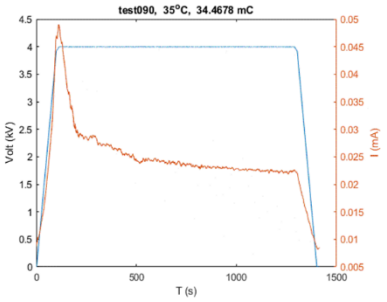

(b)

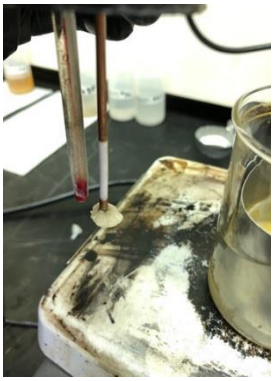

(c)

Figure 28. TN #90: 2 g PVC in 70 mL toluene, field reversed. (a) Electric current response, (b) rod with PVC deposit, and (c) convergent pattern after the test. Copper rod as HV electrode and aluminum sheet as GRD electrode; 0.8 mm thicker sediment in center; 35°C.

The posttest examination indicated the deposit took place on the rod, whereas the sheet was clean. A converging pattern, in contrast to that of TN #83, resembling a pineapple section was observed. The pattern was associated with the sedimentary layer on the bottom of the beaker. A pileup with height of about 0.77 to 0.80 mm was observed in the center, which was caused by the accumulation of particles displaced by the electric field. Thus, the movement of particles in the tested case is associated with the negatively charged particles.

5.2 DIATOMACEOUS EARTH

5.2.1 Inward Electric Field

The mixture of 2 g DE with 70 mL mineral oil was prepared for TN #84. The solutes were shown to be held well in suspension. No sediment was observed during a period of several minutes after the preparation. This state is different from the mixture of PVC and toluene in which the sediment of PVC particles occurs quickly, showing that the viscous force of oil effectively works against the gravitational force on the sediment.

The electric current response shown in Figure 29 indicates that the electric resistance of system was substantial. A radial patter emerged during the process, as seen in the image 30 min after the target voltage had reached. The particles finally settled as seen from the thick yellow layer. A posttest examination revealed a pileup of height 0.97 mm developed around the center rod. The positive charges were likely the driving mechanism for the pileup.

(a) (b) (c)

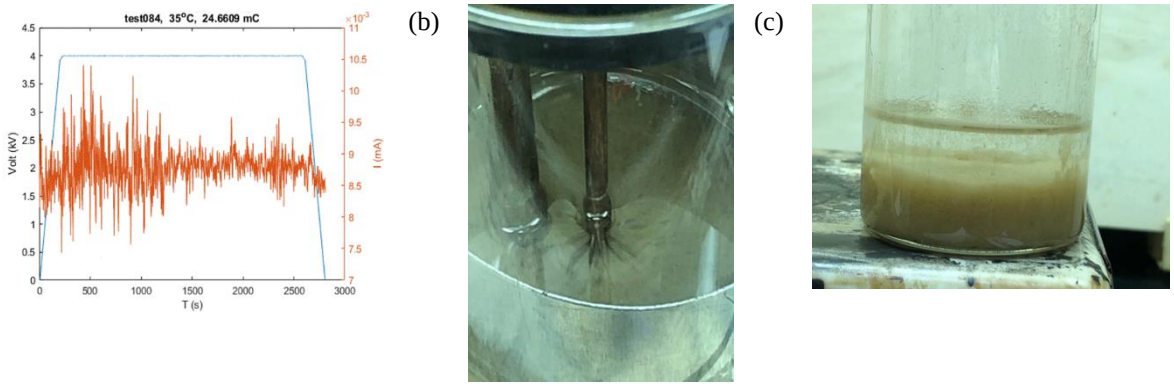

Figure 29. TN #84: 2 g DE in 70 mL mineral oil. (a) Electric current response, (b) radial pattern 30 min after target voltage achieved, and (c) settled deposit. Copper rod as GRD and aluminum sheet as HV electrode; 0.97 mm thicker deposit around rod; 35°C.

5.2.2 Outward Electric Field

A mixture with the same composition as TN #84 was prepared for TN #89. The test was conducted with reversed electric field direction (i.e., the rod as an HV electrode and the sheet as a GRD electrode). The results are illustrated in Figure 30.

(a) (b)

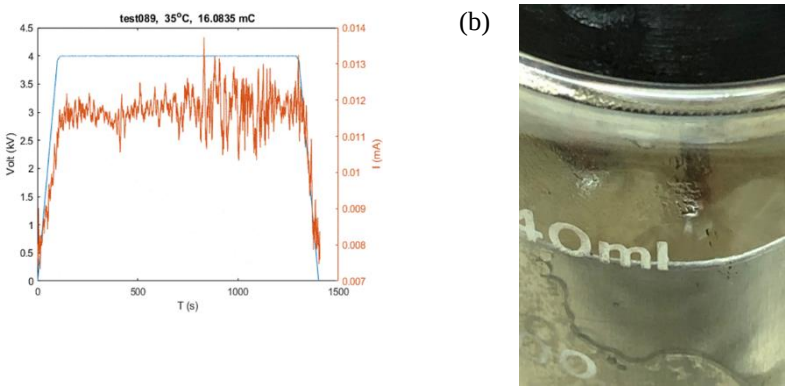

Figure 30. TN #89: 2 g DE in 70 mL mineral oil, reversed field. (a) Electric current response and (b) pattern developed in the early stage of test. Copper rod as HV electrode, sheet as GRD electrode; 3 mm thicker bottom deposit around sheet; 35°C.

The beaker used in this test had a smaller height that prevented capturing a clear picture during the test. A careful posttest examination revealed that the pileup developed around the sheet with a height of about 3 mm.

Therefore, similar to that of ESS results for CTP, the electric force on positively charged particles drove the DE particles to the sheet and produced the pileup.

5.3 DISCUSSION

5.3.1 Charge-Based Force

The driving force of particles for electrical separation of the modeling system originated from the electric charges as manifested by the directionality of the deposit under electric field. The solid particles were not electrically neutral but carried the charge.

5.3.2 Gravitational and Drag Forces

The movement of particles toward the electrode in the horizontal plane is affected by the gravitational force in the vertical direction. If the buoyancy of solid particles in the liquid is large and sustainable, then the suspension of particles will enable themselves to be subjected to a maximized action of electric force. Otherwise, the particles would quickly settle, and the effect of electric force would be compromised. For the mixture of PVC and toluene, the density of PVC is 0.575 g/cm^3 higher than that of toluene; however, the viscosity of toluene (0.59 mPa s) is fairly low (Table 7, Table 8). These created a condition for particles to settle, depending on their sizes.

The movement of particles toward the electrode in the horizontal plane is also affected by the drag force in the horizontal direction. No significant movement of particles could be induced if the electric force does not overcome drag force; therefore, no deposit would be generated. In the DE mixture with mineral oil, the viscosity (107 mPa s) (Table 8) is high compared with those of the typical fluid used in modeling system, 1 to 5 mPa s; for example, in Fang et al.[36] Even with such high viscosity, the effect of electrically-driven motion of particles was still observed as validated by the pile-ups.

5.3.3 Main Observations

- The motion of particles is originally driven by the charge-based electric force in the cases tested. The deposit depends on the electric field direction.

- The mechanical movement of solid particles can be strongly affected by the gravitational and viscous forces in the electric field.

5.3.4 Considerations for Modeling the ESS of CTP

5.3.4.1 Physical and electrical properties of CTP mixture

The literature survey indicated that no modeling system is available for ESS of CTP, but systems are available in the related applications such as FCCS. Several parameters can be predetermined, including the concentration of particles, the particle size, the dielectric properties of liquid and solid phases, and even electric charges. The density and viscosity of CTP mixtures are generally not available. Without the input, searching the solvent for modeling is difficult because the target properties are unknown. Therefore, it is necessary to conduct fundamental work to generate some preliminary data.

5.3.4.2 Upgrade of ESS setup

The test system coupled with fluid flow was also proposed and tested previously, and the results indicated that the system is effective. One concept is illustrated in Figure 31.

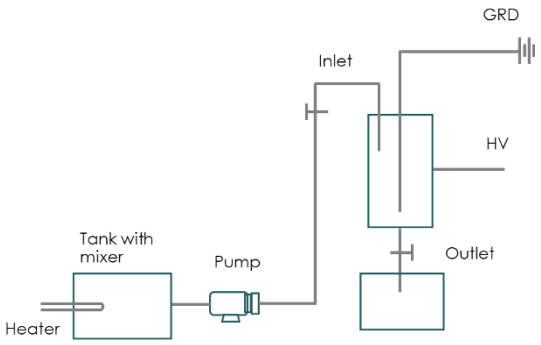

Figure 31. Electrostatic separation setup with fluid flow.

5.3.4.3 Numerical analysis of ESS

To achieve better modeling, detailed analysis of the particle forces and the effect of critical factors is needed.

6. SEM AND EDS ANALYSIS

6.1 DEPOSIT

In addition to the expected large amount of carbon and oxygen, the EDS data revealed the particles rich in sodium, aluminum, silicon, calcium, iron, and molybdenum, as shown in Figure 32 and Figure 33 for the material near the electrode disk in TN #50.

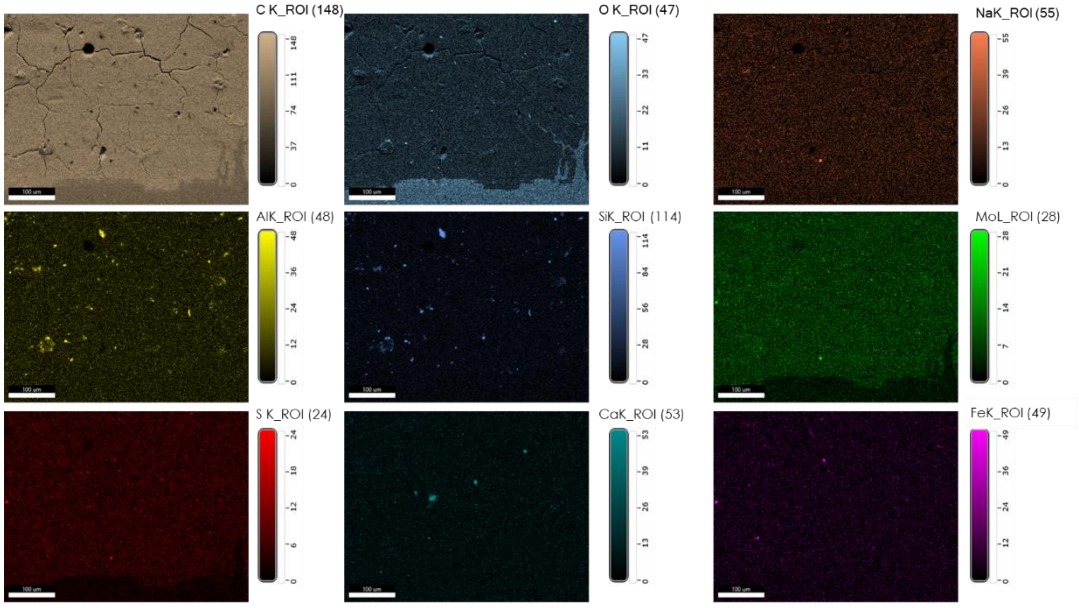

Figure 32. Element map of as-deposited sample from TN #50 near the electrode disk.

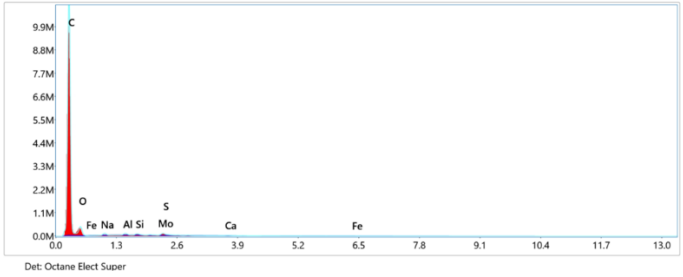

Figure 33. EDS of sample from TN #50 near the electrode disk.

The EDS analysis results are summarized in Table 19 for the materials taken from TN #50 (near the electrode disk, Koppers -80), #51 (near electrode disk, Carbores -80), #52 (near electrode rod, Koppers -80) and #63 (near electrode rod, Koppers -325).

Table 19. EDS results of deposits for various samples

TN	Solid	Liquid	Map 500X		
#50	Koppers -80	Quin.50%+Tol.50%	Element	wt %	atom %
Disk			C K	94.87	96.41
			O K	4.4	3.36
			Na K	0.2	0.11

			Al K	0.1	0.04
			Si K	0.07	0.03
			S K	0	0
			Ca K	0.03	0.01
			Fe K	0.01	0
			Mo L	0.32	0.04
#51	Carbores -80	Quin.50%+Tol.50%	Element	Weight %	Atomic %
Disk			C K	95.17	96.68
			O K	4.07	3.1
			Na K	0.15	0.08
			Al K	0.09	0.04
			Si K	0.08	0.04
			S K	0	0
			Ca K	0.03	0.01
			Fe K	0.01	0
			Mo L	0.4	0.05
#52	Koppers -80	Quin.50%+Tol.50%	Element	Weight %	Atomic %
Rod			C K	93.36	95.22
			O K	6.02	4.61
			Na K	0.1	0.05
			Al K	0.08	0.03
			Si K	0.07	0.03
			S K	0	0
			Ca K	0.03	0.01
			Fe K	0.02	0
			Mo L	0.33	0.04
#63	Koppers -325	Wash.33%+BTX33%+ETH34%	Element	Weight %	Atomic %
Rod			C K	91.26	93.55
			O K	8.12	6.25
			Na K	0.19	0.1
			Al K	0.08	0.04
			Si K	0.06	0.02
			S K	0	0
			Ca K	0.02	0.01
			Fe K	0	0
			Mo L	0.27	0.03

The detected elements were the same for Carbores and Koppers. The individual weight percent of elements is similar for both pitches. For a given pitch (e.g., Koppers), elements have a similar range of weight percent for the materials from both disk and rod areas. The detailed analysis showed that the Carbores had more carbon, silicon, and molybdenum than Koppers, as seen in Table 20. Some inorganic elements revealed in this study, such as molybdenum, were not reported previously in CTP.[55]

Table 20. Summary of EDS data for Carbores and Koppers

Map 500X	**Carbores -80**		**Koppers -80**			
Element	wt %	atom %	wt %		atom %	
			Min.	Max.	Min.	Max.
C K	95.17	96.68	91.26	94.87	93.55	96.41
O K	4.07	3.10	4.40	8.12	3.36	6.25
Na K	0.15	0.08	0.10	0.20	0.05	0.11
Al K	0.09	0.04	0.08	0.10	0.03	0.04
Si K	0.08	0.04	0.06	0.07	0.02	0.03
S K	0.00	0.00	0.00	0.00	0.00	0.00
Ca K	0.03	0.01	0.02	0.03	0.01	0.01
Fe K	0.01	0.00	0.00	0.02	0.00	0.00
Mo L	0.40	0.05	0.27	0.33	0.03	0.04

6.2 QI EXTRACTS

6.2.1 As-Prepared CTP

According to the EDS data, the QI material is mostly carbon and oxygen. The analysis of the QI extract from Carbores -80 also revealed aluminum, silicon, iron, and sulfur, as shown in Figure 34 and Table 21.

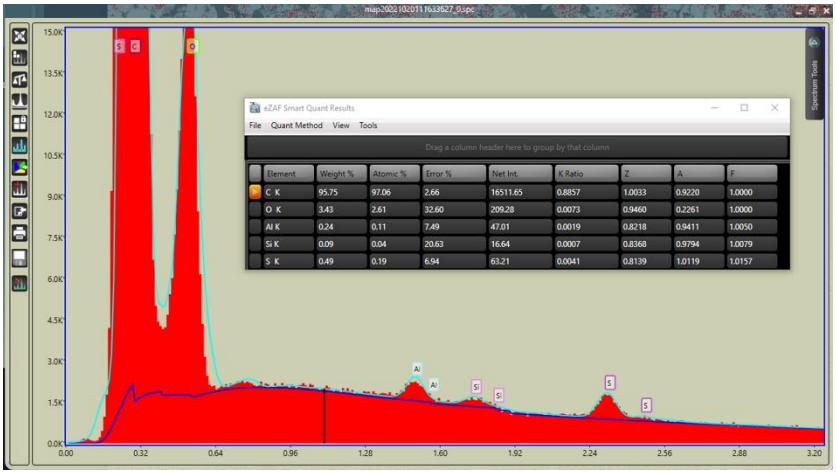

Figure 34. Area 3 of as-prepared sample, Carbores mesh -80.

Table 21. EDS results of extract based on as-prepared pitch

Area 3	**Enlarged**	Element	wt %	atom %
		C K	95.75	97.06
		O K	3.43	2.61
		Al K	0.24	0.011
		Si K	0.09	0.04
		S K	0.49	0.19
	Spot 1	Element	wt %	atom %
		C K	98.66	99.41
		O K	0	0
		Al K	1.17	0.52
		Fe L	0.01	0
		S K	0.16	0.06
Area 5	**Spot 1**	Element	wt %	atom %
		C K	98.16	98.9
		O K	1.24	0.94
		Al K	0.13	0.06
		Fe L	0.44	0.1
		S K	0.03	0.01

6.2.2 Deposit

The EDS analysis of the QI extract from the TN #48 deposit revealed sodium, aluminum, silicon, and sulfur, as shown in Figure 35 and Table 22. Therefore, the elements and weight percent ranges overlay for the QI extracts from the as-prepared pitch (w/o electrical separation; Table 21) and the deposit (Table 22). The results suggest that the composition of QI material obtained by the deposit matches that of the QI material in CTP. Therefore, the QI material of the deposit originates from the same group as that of CTP.

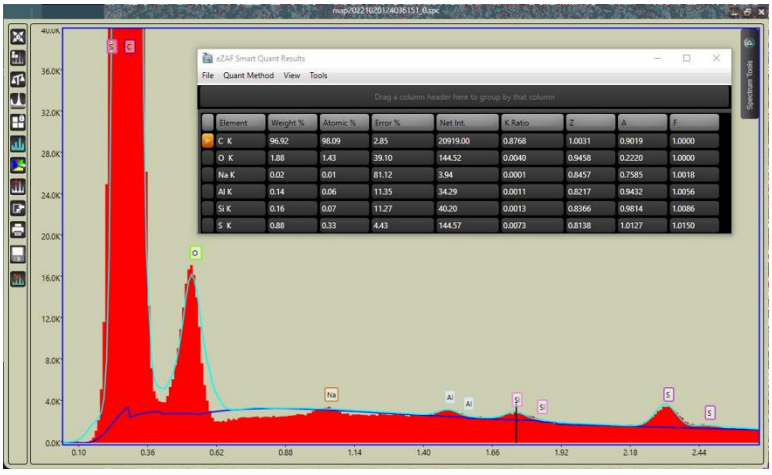

Figure 35. Area 1 of deposit extract sample, TN#48, Carbores mesh -80.

Table 22 EDS results of extract based on deposit, TN #48

Area 1	**Enlarged**	Element	wt %	atom %
		C K	96.92	98.09
		O K	1.88	1.43
		Na K	0.02	0.01
		Al K	0.14	0.06
		Si K	0.16	0.07
		S K	0.88	0.33
	Spot 3	Element	wt %	atom %
		C K	97.4	98.28
		O K	1.81	1.37
		NaK	0.3	0.16
		AlK	0.06	0.02
		S K	0.44	0.17

Not all the elements identified were included in the analysis of the QI material in the as-prepared and deposit samples, possibly introducing some variation. The presence of the individual elements and weight percentages could also arise from the uncertainty of sampling in EDS analysis.

6.3 DISCUSSION

6.3.1 Deposit

In addition to carbon, the EDS analysis revealed an appreciable amount of oxygen and small amounts of sodium, aluminum, silicon, calcium, iron, and molybdenum. The composition represents the combinational effect of QS and QI material. The oxygen is associated with the oxygen-containing molecular compounds such as the hydroxyl functional group and oxides. The metallic elements could come from the refractory bricks of the furnace, handling tools, recycling pipes, and oxide powders, as discussed by He at al.[55] Discrepancy exists between this study and the published results regarding the existence of metallic and nonmetallic elements; for example, the present study revealed molybdenum, but it was not previously reported. A full understanding of the findings must trace the source of CTPs.

The compositions obtained on all the SEM samples were consistent disregarding the location of samples taken. The Carbores contained more carbon, silicon, and molybdenum than Koppers.

6.3.2 QI Material

The chemical composition of QI material extracted from the as-prepared CTP and the deposit largely duplicated that of the deposit, particularly with respect to the metallic elements. The element sulfur was not seen in deposit but was revealed in the QI material.

Less oxygen was present in the QI material than in the deposit. This result may be caused by the removal of QS material from deposit during extraction. The difference in the oxygen weights reveals that the QS material retains some hydroxyl functional groups but is removed. Inorganic matter such as solid oxide particles likely contributes to the oxygen content in the QI material.

6.3.3 Main Observations

- The main chemical composition of deposit QI material matches that of as-prepared CTP QI material. The QI material in the deposit originates from the same population as the CTP QI material.
- In addition to carbon, the QI material contains oxygen, sodium, aluminum, silicon, iron, and sulfur.

7. SUMMARY AND FUTURE WORK

7.1 SUMMARY

This study integrated a set of experimental and analysis techniques into the electrical separation tests to investigate the feasibility of electrostatic separation of QI from CTP:

1. The study performed an extensive search and identified nine original solvents for subject CTPs, three two-part mixtures, and two three-part mixtures.
2. Test setup was modified and adapted to enhance electric field and deposit collection with the given HV capability and to examine the deposit direction as related to the electric field.
3. An extensive literature survey identified the solids and liquids for an electrical separation modeling system. Three solids and two liquids were examined.
4. QI material was extracted from both the subject CTPs and the deposits.
5. SEM and EDS were performed to analyze the chemical compositions of deposit and QI extracts.

The following is a recap of major findings and observations.

7.1.1 Electric Current Responses

- The current level of the solution of CTP–wash oil reported by Cao et al.[13] can be attained by using a mixture of quinoline and toluene for the CTPs examined in this study under same electrical load condition, namely, Quin.25%+Tol.75%.
- The electric current tends to decrease during the test period because of the decreasing quantity of charged particles.
- The reversed field corresponded to the configuration of ESP for positive corona discharge. The high electric field can cause a dielectric breakdown and lead to an abrupt current surge.

7.1.2 Deposit Response and Solvent Candidates

- Deposition of particles in the CTP mixture can be effectively implemented in a wire–cylinder configuration, as proposed and examined in this study.
- The deposit depends on the solvents. Various types of candidate solvents were examined, including single-part and multipart solvents. Among the solvents tested, two-part and three-part solvents containing quinoline and ethanol produced the highest deposit weight, including Quin.25%+Tol.75%, Quin.50%+Tol.50%, and Wash.33%+BTX33%+ETH%.
- The deposit process examined in this study originated from the charged particles. An appreciable relation exists between deposit weight and electric charge.

7.1.3 QI Removal Efficiency

- The RE of the ESP process can be as high as 76.2% for Carbores and 61.6% for Koppers.
- The RE can be further enhanced if the field level increases from 0.16 kV/mm that was used in the current study to 0.23 kV/mm, according to the relationship established between the RE and the electric field.

7.1.4 Testing of Modeling System

- The motion of particles is originally driven by the charge-based electric force in the cases tested. The solid particle separation mechanism is similar to that of QI material deposition in CTP.

- The mechanical movement of solid particles can be strongly affected by the gravitational and viscous forces in the electric field.

7.1.5 EDS Analysis and Chemical Compositions

- The main chemical composition of deposited QI material matches that of as-prepared CTP QI material. The deposited QI material originated from the same group of the CTP QI material.
- In addition to carbon, the QI material contains oxygen, sodium, aluminum, silicon, iron, and sulfur.

7.2 FUTURE WORK

7.2.1 Electrical Separation Testing

7.2.1.1 Test matrix for solvents

Additional tests to confirm the repeatability of results regarding items in the test matrix (mesh size, ratio of quinoline, electric field level; Table 10 to Table 13).

Carbores/ Koppers:

- Complete test series for Carbores: (1) Carbores -80 and toluene; (2) Carbores -325 and carbon disulfide; (3) Carbores -80 and carbon disulfide; (4) Carbores -80 and Quin.50%+USOil50%.
- Complete test series for Kopper: (1) Koppers -325 and Wash.33%+BTX33%+ETH34%; (2) Koppers -80 and Wash.33%+BTX33%+ETH34%.

Blue Gem: Additional tests are necessary to confirm whether electric separation meets the requirement.

Springfield: Need more materials.

7.2.1.2 Testing setup for high removal efficiency

- Electric field: high field level is needed to achieve 0.23 kV/mm (Table 15, Figure 25). For the existing setup, an HV amplifier with about 9 kV output is needed.
- Modification to include fluid flow: to address the potential sediment issue for practice scale-up.

7.2.2 Deposit and QI Analysis

7.2.2.1 SEM and EDS analysis of deposit

Perform systematic SEM and EDS analysis to obtain more data of deposit and QI material. For the EDS of QI material, the scans must include all the elements identified to obtain consistent weight/ atom percent data (Table 21, Table 22).

7.2.2.2 X-ray diffraction analysis and thermal analysis of deposit

- Perform XRD analysis to investigate and understand the structure of deposit.
- Perform thermal analysis to obtain thermogravimetric (TG) and differential thermal analysis curves of deposits to understand material loss response during the heating.

7.2.3 Cost Analysis

- Analyze the overall cost of removing QI material from CTP, and compare unit weight cost with counterpart methods such as the centrifugal method.
- Evaluate the cost of removing QI material and relate it to the benefit gained from enhanced performance of value-added products such as carbon fibers.

7.2.4 Numerical Modeling

Evaluate and explore the possibility of modeling particle transport in the electrical separation process.

8. REFERENCES

[1]Bhatia, G., Fitzer, E. and Kompalik, D., Mesophase formation in defined mixtures of coal tar pitch fractions, *Carbon*, **24** (4), 1986, 489-494.

[2] Mochida, I., Yoon, S.H., Takano, N., Fortin, F., Korai, Y., Yokogawa, K. Microstructure of mesophase pitch-based carbon fiber and its control, *Carbon*, **34** (8), 1996, 941–956

[3] Yang, Y., Wang, C. and Chen, M., Preparation and structure analysis of nano-iron/mesocarbon microbead composites made from a coal tar pitch with addition of ferrocene, *J. Phys. and Chem. of Solids*, **70** (10), 2009, 1344-1347.

[4] Ma, Z.H., Wei, X.Y., Liu, G.H., Liu, F.J. and Zong, Z.M., Value-added utilization of high-temperature coal tar: A review, *Fuel*, **292**, 2021, 119954.

[5] https://www.statista.com/statistics/267891/global-coke-production-since-1993, Accessed 12/14/2022

[6] Moriyama, R., Hayashi, J.I., Chiba, T. Effects of quinoline-insoluble particles on the elemental processes of mesophase sphere formation, *Carbon*, **42** (12-13), 2004, 2443–2449.

[7] Stadelhofer, J.W., Marrett, R. and Gemmeke, W., The manufacture of high-value carbon from coal-tar pitch, *Fuel*, **60** (9), 1981, 877-882.

[8] Zhu, Y.M., Zhao, X.F., Gao, L.J., Jun, L., Cheng, J.X. and Lai, S.Q., Properties and micro-morphology of primary quinoline insoluble and mesocarbon microbeads, *J. Mater. Sci.*, **51** (17), 2016, 8098-8107.

[9] Zhu, Y., Liu, H., Xu, Y., Hu, C., Zhao, C., Cheng, J., Chen, X. and Zhao, X., Preparation and characterization of coal-pitch-based needle coke (part III): the effects of quinoline insoluble in coal tar pitch, *Energy & Fuels*, **34** (7), 2020, 8676-8684.

[10] An, J.C., Lee, S.Y., Park, J.I., Ha, M., Shim, J. and Hong, I., Study of quinoline insoluble (qi) removal for needle coke-grade coal tar pitch by extraction with fractionalized aliphatic solvents and coke formation thereof, *Appl. Sci.*, **11** (7), 2021, 2906.

[11] Lei, Z., Yang, J., Hao, S., Yao, Y., Zhikun, H., Zhuorui, Z. and Hengliang, W., Purification of quinoline insolubles in heavy coal tar and preparation of mesocarbon microbeads by catalytic polycondensation, Available at SSRN: https://ssrn.com/abstract=4028744, Accessed 3/3/2023.

[12] Yu, C., Zhao, N., Guo, A., Wang, Z., Research progress in the removal of quinoline insolubles in coal tar, *Chem. Ind. and Eng. Prog.*, **34** (9), 2015, 3262-3266

[13] Cao, Q., Xie, X., Li, J., Dong, J., Jin, L., A novel method for removing quinoline insolubles and ash in coal tar pitch using electrostatic fields, *Fuel*, **96**, 2012, 314-318

[14] White, H.J., *Industrial Electrostatic Precipitation*, Addison-Wesley Publishing Company, 1963.

[15] Chang, J.S., Kelly, A.J. and Crowley, J.M., *Handbook of Electrostatic Processes*, CRC Press, 1995.

[16] Penney, G.W. and Matick, R.E., Potentials in DC corona fields. *Trans. the Amer. Inst. of Elec. Eng., Part I: Communication and Electronics*, **79** (2), 1960, 91-99.

[17] Felici, N.J., Recent advances in the analysis of the dc ionized fields-part II, *Direct Current*, **8**, 1963, 278-287.

[18] Fuchs, N., Petrjanoff, I. and Rotzeig, B., On the rate of charging of droplets by an ionic current, *Trans. the Faraday Society*, **32**, 1936, 1131-1138.

[19] White, H.J., Particle charging in electrostatic precipitation, *Trans. the Amer. Inst. of Elec. Eng.*, **70** (2), 1951, 1186-1191.

[20] Parasram, N., *Particle Motion in Electrostatic Precipitators*, Ph. D. Thesis, Imperial College of Science, 2001.

[21] Kihm, K.D., *Effects of Nonuniformities on Particle Transport in Electrostatic*, Ph. D. thesis, Stanford Univ., CA (USA), 1987.

[22] Riehle, C. and Loffler, F., Investigations of the particle dynamics and separation efficiency of a laboratory-scale electrostatic precipitator using laser-doppler velocimetry and particle light-scattering size analysis. In *Proc. the Fourth Int, Conf, on Electrostatic Precipitation*, Sept. 1990, pp. 136-158.

[23] Kim, S.H. and Lee, K.W., Experimental study of electrostatic precipitator performance and comparison with existing theoretical prediction models, *J. Electrostatics*, **48** (1), 1999, pp.3-25.

[24] Long, Z. and Yao, Q., Evaluation of various particle charging models for simulating particle dynamics in electrostatic precipitators, *J. Aerosol Sci.*, **41** (7), 2010, pp.702-718.

[25] Cottrell, F.G., Art of separating suspended particles from gaseous bodies, *U.S. Patent* 895,729, 1908.

[26] Yan, K. ed., *Electrostatic Precipitation*: 11th international conference on electrostatic precipitation, Hangzhou, 2008. Zhejiang Univ. Press & Springer, 2010.

[27] Pohl, H.A., Some effects of nonuniform fields on dielectrics, *J. Appl. Phys.*, **29** (8), 1958, 1182-1188

[28] Pohl, H.A., *Dielectrophoresis: the behavior of neutral matter in nonuniform electric fields*, December 29, 1978, Cambridge University Press, Cambridge

[29] Pohl, H.A, Schwar, J.P., Factors affecting separations of suspensions in nonuniform electric fields, *J. Appl. Phys.*, **30** (1), 1959, 69-73

[30] Chen, K.W.-L. L., Diele*ctrophoresis of Solids in Aqueous Solutions*, M.S. Thesis, Oklahoma State University, Aug. 1969

[31] Feeley, C.M., *Dielectrophoresis of Solids in Liquids of Differing Dielectric Constant and Conductivity*, M.S. Thesis, Oklahoma State University, Aug. 1969

[32] Chen, C.-S., Pohl, H.A., Huebner, J.A., and Bruner, L.J., Dielectrophoretic precipitation of silver bromide suspensions, *J. Colloid and Interface Sci.*, **37** (2), 1971, 354-363

[33] Benguigui, L., & Lin, I. J. Dielectrophoretic filtration of nonconductive liquids, *Separation Sci. and Technol.*, **17** (8), 1982, 1003-1017

[34] Fang, Y.J., Xiao, W.D., Wang, G.R., Study on electrostatic separation of solid-liquid systems, I. Cold model experiment, *Petrochem. Technol.*, **27** (1), 1998, 69-72

[35] Fang, Y.J., W.D. Xiao, and G.R. Wang, Study on electrostatic separation of solid-liquid systems II. Measurement of saturated adsorption weigh, *Petrochem. Technol.*, **27** (11), 1998, 815-818

[36] Fang, Y. J., W.D. Xiao, and G.R. Wang, Study on electrostatic separation of solid-liquid systems III. Hot model experiment, *Petrochem. Technol.*, **28** (5), 1999, 312-315

[37] Guo, A. Gong, L. Zhao, N., Chen, K., Liu, H., Wang, Z., Huang, J., Sun, M. Yuan, J., The influence of additive modification on electrostatic separation of FCC slurry oil, *Chem. Ind. and Eng. Prog.*, **36** (9), 2017, 3266-3272

[38] Li, Q., Wu, Z., Zhang, Z., Wang, Z. Guo L., & Li A., Experimental study on the removal of FCCS catalyst particles by electrostatic separation, *Energy Sources, Part A: Recovery, Utilization, and Environmental Effects*, 2019, DOI:10.1080/15567036.2019.1668505

[39] Li, Q., Cao, H., Qiu, Q., Guo, L., Li, A., Xu W., & Wang Z., Experimental study on the removal of FCCS catalyst particles by the coupling interaction of the electrostatic field and flow field, *Petrol. Sci. and Technol.*, 2022, DOI:10.1080/10916466.2022.2060255

[40] Li, Q., Cao, H., Qiu, Q., Yang, H., Li, A. and Wang, Z., Effect of stacking method of fillers on the electrostatic separation performance of FCC slurry, *Advanced Powder Technol.*, **33** (2), 2022, 103401.

[41] Fritsche, G.R. and Stegelman, A.F., Electrostatic catalyst separator upgrades FCC bottoms, *Oil Gas J.*, **78** (40), 1980, 55- 59.

[42] Wang, H., and Wereszczak, A. A., Effects of electric field on the biaxial strength of poled PZT, Proc. the 31st Int. Conf. on Adv. Ceramics and Composites, Jan. 21-26, 2007, Daytona Beach, FL, also in Advances in Electronic Ceramics, *Ceram. Eng. Sci. Proc.*, **28** (8), 2007, 57-67

[43] Wang, H. and Wereszczak, A. A. Effects of electric field and biaxial flexure on the failure of poled lead zirconate titanate, *IEEE Trans. Ultras. Ferroelec. Freq. Contr.*, **55** (12), 2008, 2559-2570.

[44] Wang, H., Matsunaga, T. and Lin, H.T., Characterization of poled single-layer PZT for piezo stack in fuel injection system. Proc. the 34th Int. Conf. on Adv. Ceramics and Composites, Jan. 24-29, 2010, Daytona Beach, FL, also in Mechanical Properties and Performance of Engineering Ceramics and Composites V, *Ceram. Eng. Sci. Proc.*, **31** (2), 2010, 127-136

[45] Wang, H. Lin, H.-T. and Wereszczak, A. A. Strength properties of poled lead zirconate titanate subjected to biaxial flexural loading in high electric field, *J. Am. Ceram. Soc.*, **93** (9), 2010, 2843-2849.

[46] Zhang, K., Zeng, F. W., Wang, H., and Lin, H.-T., Strength properties of aged poled lead zirconate titanate subjected to electromechanical loadings, *Smart Mater. Struct.*, **21**, 2012, 117001.

[47] Zhang, K., Zeng, F. W., Wang, H., Lin, H.-T., Biaxial flexural strength of poled lead zirconate titanate in high electric field with extended field range, *Ceramic International*, **39** (2), 2013, 2023-2030.

[48] https://depts.washington.edu/eooptic/linkfiles/dielectric_chart%5B1%5D.pdf, Accessed 12/14/2022

[49] Wohlfarth, Ch. Dielectric constant of quinoline, *Landolt-Börnstein - Group IV Physical Chemistry*, **17**, M.D. Lechner (ed.), SpringerMaterials, 2008, https://materials.springer.com/lb/docs/sm_lbs_978-3-540-75506-7_279, Accessed 12/14/2022

[50] Carey, A.A, Hayzen, A.J., Dielectric constant and oil analysis, https://www.machinerylubrication.com/Read/226/dielectric-constant-oil-analysis, Accessed 12/14/2022

[51] Coronel C., E. A., Physicochemical and infrared spectral properties of biodiesel fuels synthesized from some vegetable oils, *Revista Boliviana de Química*, **28** (1), 2011, 41-45

[52] Anton Paar, Viscosity of Toluene, https://wiki.anton-paar.com/us-en/toluene/, Accessed 12/14/2022

[53] Marko, M.D., Kyle, J.P., Wang, Y.S.; Terrell, E. J., Mineral oil dynamic viscosity data. PLOS ONE. Figure. 2017, https://doi.org/10.1371/journal.pone.0175198.g008, Accessed 12/14/2022

[54] ASTM D2318-20, Standard Test Method for Quinoline-Insolubles (QI) Content of Tar and Pitch, ASTM International, West Conshohocken, PA, June 2020.

[55] He, X., Liu, D., Wang, Y., Chen, Y., Zhang, H., Analysis and characterization of quinoline insoluble in coal tar, *Materials Reports B*, **31** (11), 2017, 142 -145